

UNIVERSIDAD AUTÓNOMA DE NUEVO LEÓN
FACULTAD DE CIENCIAS FÍSICO-MATEMÁTICAS



TESIS

ON AERODYNAMICS OF BASEBALL PITCHES:
RECONSTRUCTION OF SPINNING THROWS, AND A
LIFT FORCE MODEL FOR THE KNUCKLEBALL

POR

MARIO ALBERTO AGUIRRE LÓPEZ

SOMETIDA PARA OBTENER EL GRADO DE
MAESTRÍA EN CIENCIAS CON ORIENTACIÓN EN
MATEMÁTICAS

DICIEMBRE 2016

UNIVERSIDAD AUTÓNOMA DE NUEVO LEÓN
FACULTAD DE CIENCIAS FÍSICO-MATEMÁTICAS
CENTRO DE INVESTIGACIÓN EN CIENCIAS FÍSICO-MATEMÁTICAS



TESIS

ON AERODYNAMICS OF BASEBALL PITCHES:
RECONSTRUCTION OF SPINNING THROWS, AND A
LIFT FORCE MODEL FOR THE KNUCKLEBALL

POR

MARIO ALBERTO AGUIRRE LÓPEZ

SOMETIDA PARA OBTENER EL GRADO DE
MAESTRÍA EN CIENCIAS CON ORIENTACIÓN EN
MATEMÁTICAS

UNIVERSIDAD AUTÓNOMA DE NUEVO LEÓN
FACULTAD DE CIENCIAS FÍSICO-MATEMÁTICAS
CENTRO DE INVESTIGACIÓN EN CIENCIAS FÍSICO-MATEMÁTICAS

Los miembros del comité de tesis de la subdirección de posgrado de la Facultad de Ciencias Físico-Matemáticas, recomendamos que la tesis “On Aerodynamics of Baseball Pitches: Reconstruction of Spinning Throws, and a Lift Force Model for the Knuckleball” realizada por el Ing. Mario Alberto Aguirre López, con número de matrícula 1443147, sea aceptada para su defensa para opción al grado de Maestría en Ciencias con Orientación en Matemáticas.

El Comité de Tesis

Dr. Francisco Javier Almaguer Martínez

Asesor

Dr. Javier Morales Castillo

Co-asesor

Dr. Gerardo Jesús Escalera Santos

Co-asesor

Vo. Bo.

Dr. José Fernando Camacho Vallejo

Coordinador del Posgrado en Ciencias con Orientación
en Matemáticas

Abstract

On Aerodynamics of Baseball Pitches: Reconstruction of Spinning Throws, and a Lift Force Model for the Knuckleball

Baseball pitchers have a wide repertory of throws, which can be classified in two types: spinning and non-spinning balls. Dynamics of spinning balls is widely understood while only a few works about non-spinning balls are found in literature. On the other hand, there are some methods to reconstruct baseball trajectories, however, these methods do not usually deal with the movement equations, and if they do, its by knowing a lot of points of the real trajectory.

This work consists of two parts, both of them focused on real baseball pitches. In the first part, a method to reconstruct trajectories by obtaining the initial conditions (velocity and angular velocity) from spinning throws is designed. It is based on considering Magnus effect can be separate from rest of forces that define the dynamics of the ball, such assumption is supporting by an energetic analysis. Thus, methodology consist in solving the two-point boundary value problem (BVP) of the movement equations without the Magnus force and then adding its effect. The second part deals with the lift force present in knuckleball pitches, which is caused by the asymmetries on the ball morphology and has an oscillatory behavior varying the seams orientation. We propose a model to compute said force for two-seams (2S) and four-seams (4S) orientations, by means of a coefficient (lift coefficient) depending on the positions of each stitch of the ball seams.

As a result from the knuckleball study, a lift coefficient model is constructed by fitting a function to experimental data reported in literature. Deflections in knuckleball trajectories are calculated as a complement. Regarding spinning pitches, analyses mentioned above lead us to assume that only three points (ball position in function of time) for a trajectory to reconstruct all it. This is applied in an algorithm based on shooting method, which obtains the initial conditions of synthetic trajectories with a high accuracy in a low-time.

Acknowledgements

First of all, I want to thank to God, family and friends, for many things but mainly for helping me and putting up with me in all time.

I thank my mentors Roberto Soto and Javier Almaguer. Throughout the four years or more that I have to know them, they have encouraged and supported me to move forward, but moreover, they always have believed in me.

Next, I wish to express my gratitude to two professors from whom I'm sure I have learned more out of the classroom than inside it. Many thanks to the Dr. Javier Morales for sharing his work experiences, showing interested in the ideas I propose, and constantly reminding me about looking for ways to improve a work. Concerning my dear friend, Dr. Gerardo Escalera, this work wouldn't consist of two parts if he had not been involved in it but over all, I thank him for his hospitality and for listening and giving me his advice about many things; I'm honored to meet and work with him.

I also show gratitude to Dr. Orlando Díaz, who takes part of this research, Dr. Idrish Huet and Dr. Claudio Contreras, who expressed interest in this work and contributed to it with some interesting ideas, as well as my friend Celina Torres, who made the English language corrections of this manuscript.

Last, I want to mention that I have been benefited in several ways by the *Posgrado en Ciencias con Orientación en Matemáticas* of the *Facultad de Ciencias Físico-Matemáticas* of the *Universidad Autónoma de Nuevo León*, the *Facultad de Ciencias Física y Matemáticas* of the *Universidad Autónoma de Chiapas*, and the CONACyT.

Mario Alberto Aguirre López

Why Baseball?

About a year ago, I came back home thinking about a class project related to the use of ink-jet systems in the printing expiration labels on bottled products. It consisted on measuring the deflection of the ink drops passing through an electric field to correct the enlargement on the ends of the label. Meanwhile, my brothers were watching a baseball game on TV, and then I asked to myself: Isn't that the same effect as when the pitcher throws a spinning ball?

This led me to the idea of analyzing baseball's dynamics to design a method to reconstruct trajectories with applicability on pitching machines.

Contents

Abstract	iii
Acknowledgements	iv
Contents	vi
1 Introduction	1
1.1 Summary	3
1.2 Aerodynamics of Spinning Pitches	6
1.3 Concerning Knuckleballs	10
1.4 Reconstruction of Trajectories: Background	11
2 Calculation of the Magnus Effect on Spinning Pitches	12
2.1 Equations of Motion	12
2.2 Simulation of Throws	15
2.3 Final Deflection as Function of the Angular Velocity Components	16
3 Reconstruction of Trajectories	19
3.1 Energetic Analysis of the Movement Equations	19
3.2 The Method for Reconstructing Trajectories	21
3.3 Results	26
4 The Knuckleball	30
4.1 Lift Force Model for 4S and 2S Ball Orientations	30
4.2 Results and Knuckleball Trajectories	32
5 Conclusions	36
Bibliography	37

*To God and to my beloved family:
dad, mom, Rober and Fer*

Chapter 1

Introduction

Appreciation for baseball is a matter of taste. A lot of people refer to it as a very boring game, nevertheless it's one of the most popular sports in North America (United States, Canada and Mexico), the Caribbean (Cuba, Dominican Republic, Puerto Rico, among others), South America (Venezuela and Colombia) and Asia (Japan and South Korea).

This is probably because for a non-fan, baseball may seem less dynamic in comparison with other sports (i.e soccer, basketball). In fact, the prolonged nature of the game, along with just a few moments of excitement through it and the interaction of apparently just two of the players (pitcher and catcher) is what people who is not into this sport think baseball is about.

But then, what makes people fall in love with baseball? A part of the answer is maybe related to “the expectation”. On every pitch and every swing there is the expectation of a home run, a base stealing, a strike, or simply to listen the sound of a hit ball. All in all, there are so many emotion moments seem there are none.

Even so, baseball has a second aspect to win the heart of lots of people, this aspect inspired Albert Einstein to rename the “American pastime” as the “king of the sports”, by saying: *“You teach me baseball and I'll teach you relativity ... no we must not. You will learn about relativity faster than I learn baseball”*, after he seeing Major League Baseball game at the Yankee Stadium. The fact is that at that game, he realized that there are a lot of variables involved in this sport and how unpredictable it becomes, because nothing is solved until the last out. This is the magic of the baseball.

In more detail, Einstein observations refer to both the structure of the game and the physics involved in it. A small variation on the initial velocity, the direction or the orientation of

the ball can cause it deviate from its original trajectory by millimeters and this could be the difference between a strike, a foul ball or a even home run [1]. This is way people inside the world of the baseball always have been aware of the physics behind this sport.

Now, we get to the main point of this thesis: the physics of pitching a ball. Pitching is one of the most important events of the game, whereby pitchers must be very careful choosing their repertory of throws. These throws can be classified in two groups, depending on the relative motion of the ball in relation to its center of mass: throws with big spins - like curveballs, sliders, change-ups and fastballs - and the only throw that doesn't have an initial spin, the knuckleball¹.

Considering the baseball by its center of mass, the dynamics of both groups of pitches can be represented by Newton's second law [2, 3], so that

$$m\dot{\mathbf{V}} = \mathbf{F}_B + \oint_S \sigma dS \cdot \hat{\mathbf{n}}, \quad (1.1)$$

where the first term on the right side represents the gravitational force (\mathbf{F}_g), the Coriolis force (\mathbf{F}_{cor}) and the centrifugal force (\mathbf{F}_{cf}),

$$\mathbf{F}_B = \mathbf{F}_g + \mathbf{F}_{\text{cor}} + \mathbf{F}_{\text{cf}}, \quad (1.2)$$

whereas the second term is the net force acting across the surface S of the ball, thus covering the air-ball interaction of the throw [3].

In contrast with forces acting through the volume of the ball (those in equation (1.2)), it's difficult to write a general expression for aerodynamic forces, since the stress tensor σ change significantly for rotating and non rotating balls so that we could say only drag force (\mathbf{F}_d) plays an important role to be considered in the aerodynamics of both types of pitches.

Moreover, high angular frequencies present in spinning throws originate a difference of pressure on the sides of the ball, causing a movement of its center of mass towards the low pressure region [1]. This phenomenon is connected to the existence of the so-called Magnus force (\mathbf{F}_M), which is the distinctive effect of spinning pitches [4–6]. On the other hand, angular velocities below ~ 5 rad/s in knuckleballs [7] allow the seams of the ball to play the most important role in the ball's aerodynamics. As a consequence, asymmetric turbulent layers and laminar boundary layers appear on different sides of the ball, which originate lift (\mathbf{F}_{L_f}) and lateral (\mathbf{F}_{L_t}) forces that are not fully understood.

¹Although in real life knuckleball pitches have an initial spin, the ball rotation is not enough for it to be considered a rotating ball.

1.1 Summary

As a general overview, baseball is played in a field with shape of diamond, which is divided in two parts, outfield and infield. See the top schematic in Figure 1.1. The action of pitching is carried out at a mound in the center of the infield, where the pitcher's plate is located. The pitcher throws the ball to the home plate (in mound-home direction) as the one represented in the bottom schematic of Figure 1.1. In this way, the axes are defined as next: y -axis is fixed in direction mound-home, being z -axis perpendicular to the Earth's surface, and x -axis orthogonal to both y and z axes, according to the right hand rule.

This thesis is focused on professional baseball pitches. Some assumptions strongly depend on the initial conditions: velocity $\mathbf{V} \equiv (V_x, V_y, V_z)$ and angular velocity $\boldsymbol{\omega} \equiv (\omega_x, \omega_y, \omega_z)$, inside the range of a professional throw, namely, $\mathbf{V} \in [(-3, 30, -3), (3, 50, 3)]$ m/s, $|\boldsymbol{\omega}| \in [100, 310]$ rad/s for spinning pitches [8], and $\mathbf{V} \in [(-3, 20, -3), (3, 40, 3)]$ m/s, $|\boldsymbol{\omega}| \in [0, 5]$ rad/s for knuckleballs [7], taking the system of axes mentioned in last paragraph.

The research consists of two parts:

- The first part is about the design of a method to reconstruct trajectories by obtaining the initial conditions of spinning throws, taking into account the movement equations of the center of mass of the ball. The methodology used is the following: In accordance to the studies shown in Section 1.2, approximation of the forces on the left-hand side of Figure 1.3 are used to compute the movement equations (Section 2.1). They are solved numerically to define some of the relations between the angular velocity and the final position of the ball (Section 2.2 and 2.3). An energetic analysis of the equations of motion is carried out in Section 3.1 to support those assumptions. All of this is compiled in the design of the solution method in Section 3.2.
- The second part deals with the aerodynamics of non rotating balls. We compiled experimental and analytic studies about lift force present in knuckleballs - Section 1.3 - to construct a mathematical model that can compute this force for 4S and 2S ball orientations by means of a coefficient (the lift coefficient) that considers the effect caused by each stitch on the ball seams (Chapter 4). Thus, the lift coefficient can be computed in function of the initial angle of the ball (see Figure 1.2). In turn, this permits us to complete the movement equations of non rotating baseballs according to the diagram of forces shown on the right-hand side of Figure 1.3 and consequently, to reproduce knuckleball trajectories.

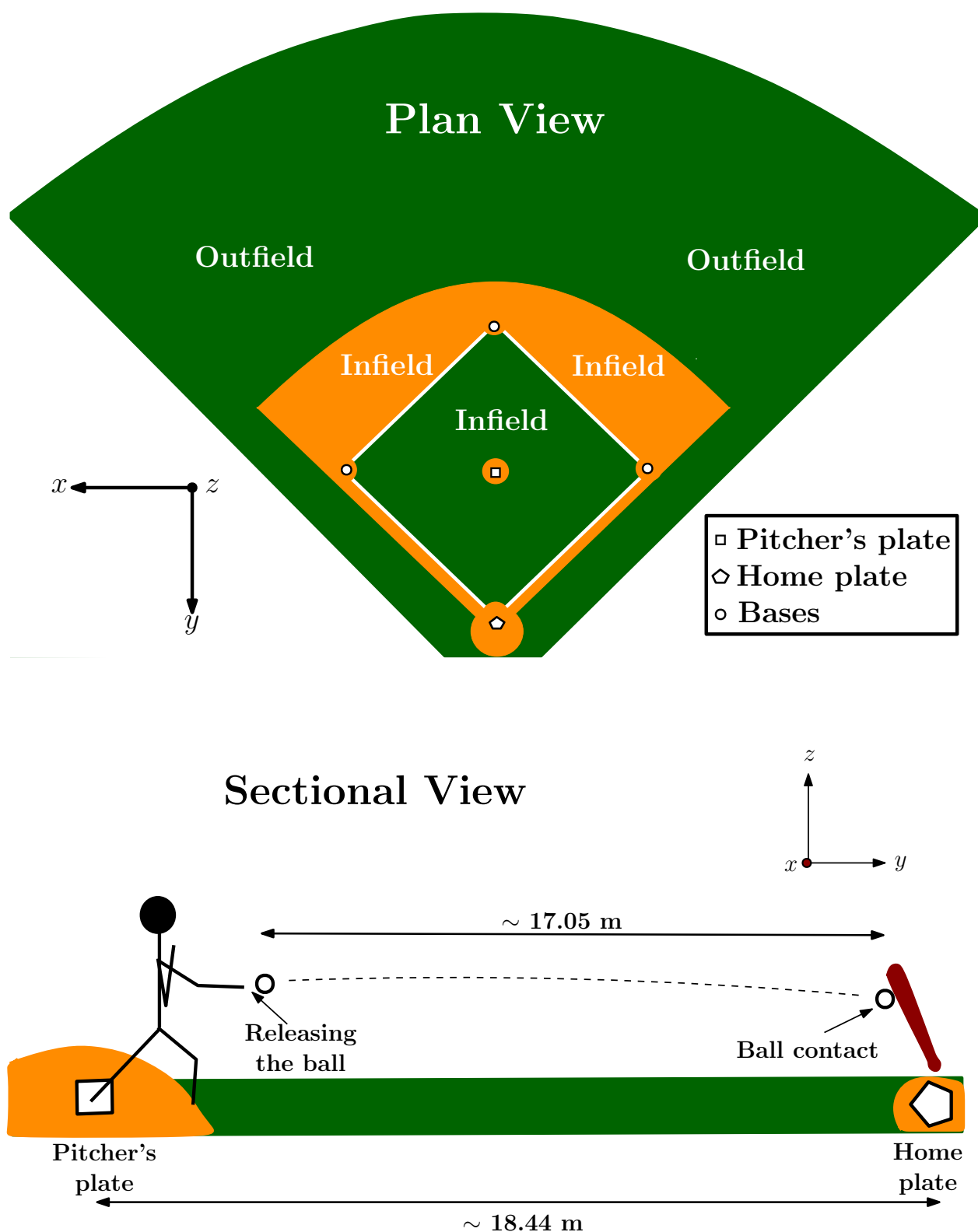


FIGURE 1.1: Schematics of a baseball field (not scaled). Up: Plain view of a complete baseball field. The layout indicates the division of the field as well as the positions of bases and home and pitcher's plates. Bottom: Sectional view of the mound-home zone. Distance between the pitcher's plate and the home plate is around 18.44 m, in accord to the *Official Baseball Rules* [9], however, the distance between the point in which the pitcher release the ball and that where the bat hits the ball is around 17.05 m [1].

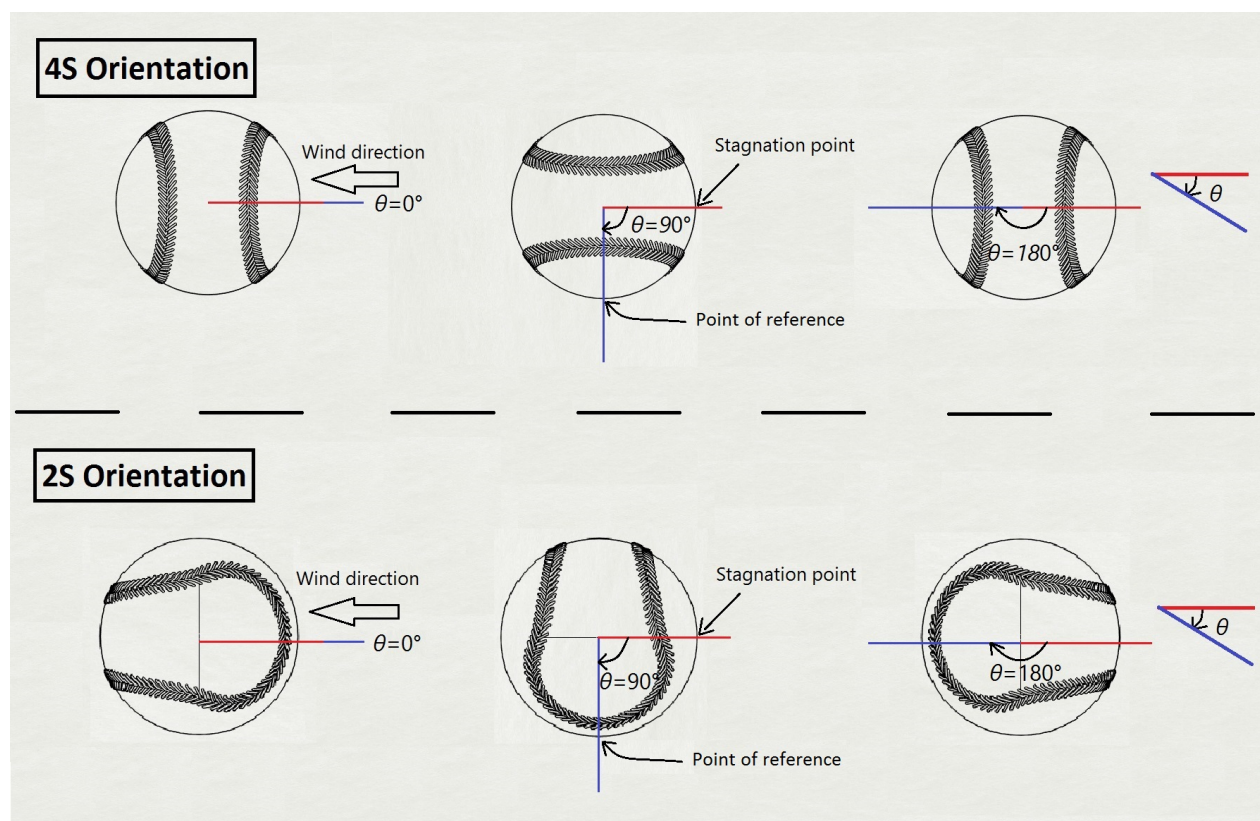


FIGURE 1.2: Schematic of knuckleball orientations. A ball is thrown to the right without rotation at different angles θ . The angle is measured from the point of stagnation (red line) to the point of reference of the ball (blue line). Up: Four seam (4S) orientation. Bottom: Two seam (2S) orientation.

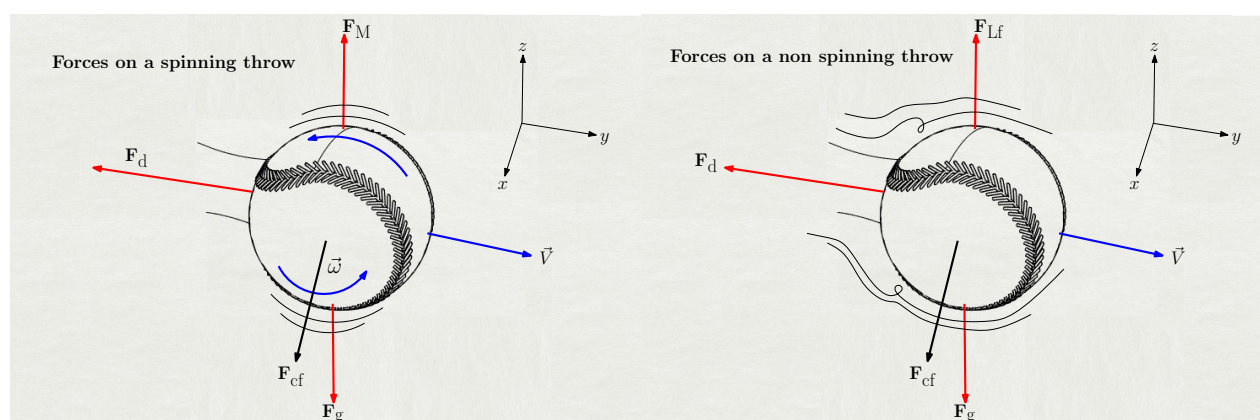


FIGURE 1.3: Diagram of forces for rotating and non rotating baseballs. In both cases, drag (\mathbf{F}_d) and Earth forces (gravitational (\mathbf{F}_g) and centrifugal (\mathbf{F}_{cf}) forces) are present. In addition, spinning throws (left) are affected by Magnus force (\mathbf{F}_M), whereas deflections in the trajectory of non spinning throws (right) are caused by the air-seams interaction, which is involved in the lift force (\mathbf{F}_{Lf}). Note: The centrifugal force is a fictional force.

1.2 Aerodynamics of Spinning Pitches

Drag Force

Drag (or friction) is maybe the most well-known consequence of the air-ball interaction. In general, any object moving through the air receives a force in opposite direction of its motion with magnitude in function of the velocity \mathbf{V} of its center of mass, i.e.,

$$\mathbf{F}_d = -F_d(V)\hat{\mathbf{V}}. \quad (1.3)$$

Such phenomenon is explained by the conservation of momentum. The medium is non empty since there are air molecules that oppose resistance to the pass of the ball in the manner of tiny particles therefore, a difference of pressure between front side and back side of an object is occasioned when it flies throughout the air. As shown in both diagrams of Figure 1.4, stream lines on the back side of the ball are farther than on the front side (for both, rotating and non rotating balls). This creates a low pressure region in the back side of the ball that causes a momentum with reverse direction to its motion [1, 2, 10].

Now, the question is how are related the difference of pressure and the drag force magnitude (F_d). At first, it's not difficult to think that air conditions, and the shape and the speed of the ball are involved in such ratio. Indeed, experimental data [1, 6, 11] suggest an approximation proportional to the square of the ball speed, so that

$$F_d \approx \frac{1}{2}\rho AC_d V^2 \quad (1.4)$$

where factor $\frac{1}{2}\rho V^2$ is the difference of pressure between the front side and the back side (with ρ the air density) that exist considering the ball has a transverse section front area A [10]. In turn, C_d is a dimensionless coefficient that is introduced because the interaction between the front area and the stream lines decreases when the speed of the ball V increases, i.e., the effective front area decreases, making the ball more aerodynamic.

In this way, drag coefficient can be written in function of the ball speed ($C_d \equiv C_d(V)$), but spiting this, it's commonly taken like a constant [5, 6]. The values of the lift coefficient are estimated by Adair [1] considering the average of experimental values for all types of pitches and measures of baseballs in free fall, see the left-hand side of Figure 1.5.

Moreover, experimental measures, model (1.4) is supported by Reynolds number approximating F_d with a Taylor series. Baseballs with diameter d inside the limits established by *Professional Baseball Rules* [9], $d \in [7.27, 7.48]$ cm, moving at standard air conditions with

initial velocities proposed in Section 1.1, $V \in [30, 50]$ m/s, produce Reynolds numbers Re in the order of $3.5 \times 10^3 - 6 \times 10^3$ which correspond to the laminar-turbulent transition flow of air [6]².

Then, in order to approximate F_d in equation (1.3) by the Taylor series

$$F_d(V) \approx k_1 + k_2V + k_3V^2 + \dots + k_{n+1}V^n, \quad (1.5)$$

$Re \in [3.5 \times 10^3, 6 \times 10^3]$, the size of the ball and the boundary condition $F_d(0, k) = 0$ allow the third term to be the only one remaining of the summation in (1.5), as in equation (1.4). Additionally, according to Taylor [2], at standard air conditions it's possible define a ratio between linear f_{lin} and quadratic f_{quad} terms depending on the velocity V and diameter d of the ball, such that

$$\frac{f_{quad}}{f_{lin}} = \left(1.6 \times 10^3 \frac{\text{S}}{\text{m}^2}\right) Vd > 2000$$

which means that a quadratic drag force delay the flight of the ball approximately 2000 times more than a linear drag force approximation. This result is reflected at the end of the trajectory as is shown in Table 2.1 in Chapter 2, where the estimation of the deflection produced by a quadratic drag approximation is around one-two meters; thus, a linear approximation will produce deflections below one millimeter, which are considered negligible [1].

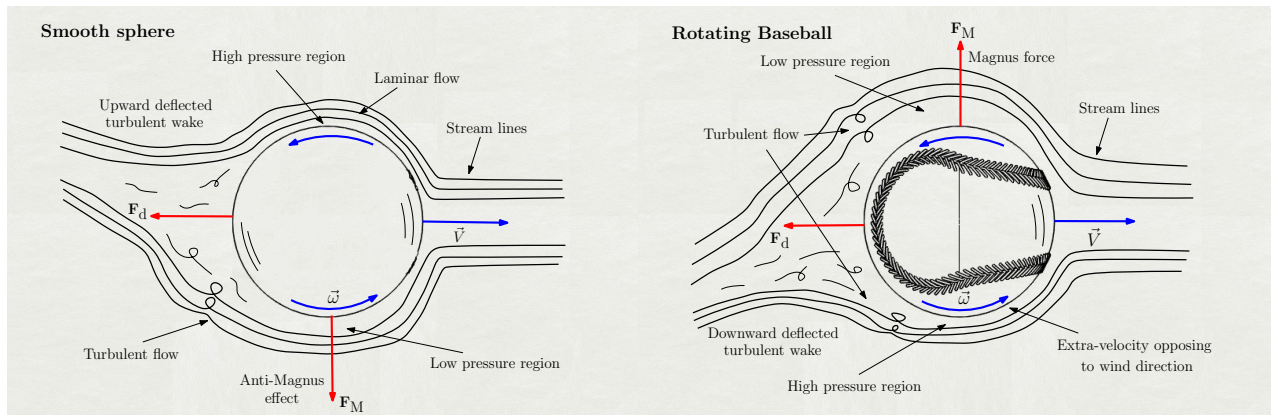


FIGURE 1.4: Schematic showing the stream lines of two spinning balls moving to the right of the page with an angular velocity ω . Left: Laminar flow on the upside of a smooth sphere produce a high pressure region and allows the ball to experiment the anti-Magnus effect. Right: A baseball rotating in the same direction of the smooth sphere has an upward motion (the normal Magnus effect) caused by the difference of velocities on its up-down sides. Based on the schematic diagram of Robinson & Robinson [6].

²This result is applicable, considering the ball like a smooth sphere. Moreover, roughness of the baseball and high spins increment the Reynolds number to values in the order of 10^6 , which correspond to a more turbulent flow [1].

Magnus Force

Magnus force is the second main aerodynamic force present in spinning throws. All of us have a clear empirical knowledge of its effect in any rotating ball (like in soccer [12], cricket [6, 13] and tennis [14]): large changes in the trajectory of a moving ball are reached by increasing the spin frequency. Although this assumption is true, the direction caused by the deflection could vary in some cases. Indeed, a reverse direction of Magnus force (anti-Magnus effect) has been reported for smooth balls like those used in soccer games [12], and in smooth spheres simulating baseballs in Briggs experiments [4] and references therein.

According to Briggs [4], it is possible only for a range of Re when one side of the smooth ball remains in a laminar flow while the opposite side becomes turbulent. Then, a low pressure region is originated in the turbulent side because it is generally farther to the ball surface than the laminar layer. Thus, the ball moves to the region with lower pressure by conservation of momentum, see left-hand of Figure 1.4.

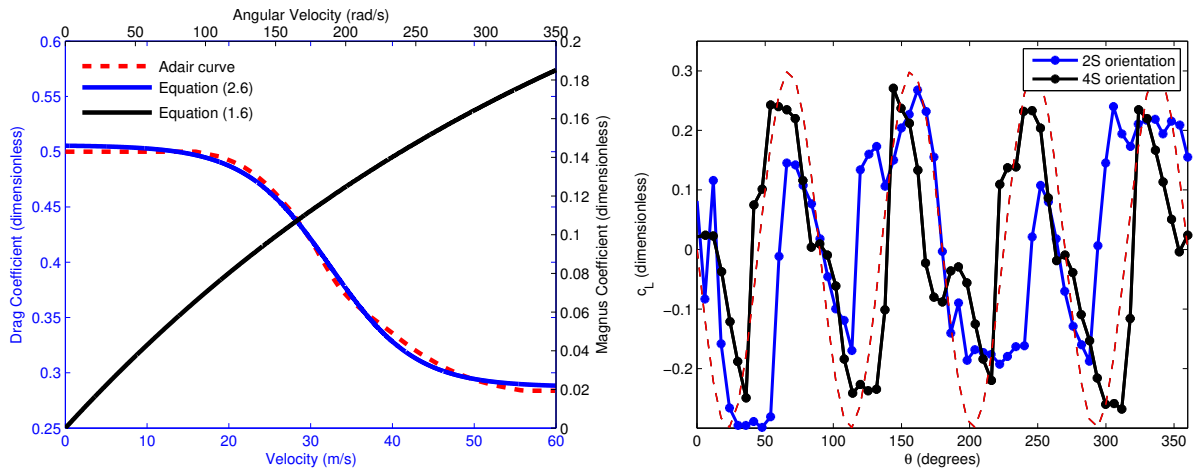


FIGURE 1.5: Left: Drag (C_d) and Magnus (C_M) coefficients. The red dashed line represents the Adair estimation for C_d . The blue solid line approximates Adair curve by equation (2.6), while black line fits to the Briggs experimental data using equation (1.6). Right: Lift coefficient (C_{Lf}) measures of Borg & Morrissey as a function of the initial angles $\theta \in [0^\circ, 360^\circ]$ for baseballs with 4S and 2S orientations. Equation (4.2) with $a_0 = 0.3$ (red dashed line) is plotted as a baseline. Both Adair and Borg & Morrissey data were extracted using tools of Matlab R2013a program.

However, this is not the case of typical baseballs, whose seams don't permit a constant laminar flow on any side of it. Conversely, when a rough ball flies, spinning through the air, a side of it opposes to the air force causing a bigger resistance than in the opposite side, i.e. air velocity on the up side is lower than in the bottom side, according to the right-hand side of Figure 1.4. Then, since low velocities are associated with high pressure regions and vice versa [15], a low pressure region is originated at the top of the ball, which leads to the normal Magnus effect [1, 6].

Similarly to drag force, experimental measures [4, 5] indicate that Magnus force acting in upward direction can be written as $F_M \approx \frac{1}{2}\rho AC_M V^2$ with the adaptive dimensionless coefficient of area C_M in function of ω and V [1, 5]. Even more, experimental studies of Nathan [5] show that C_M (the Magnus coefficient) depends mainly on the angular velocity, for ω and \mathbf{V} values inside the range mentioned in Section 1.1. This permits to complete the model expressing the Magnus coefficient by the exponential relation

$$C_M(\omega) = 3.19 \times 10^{-1} \left[1 - e^{-2.48 \times 10^{-3} \omega} \right] \quad (1.6)$$

which originally was employed to fit C_M values for golf balls, but that is also close to experimental data reported by Briggs [4], as mentioned in Robinson & Robinson works [6, 17]. Expression (1.6) is plotted by the black curve in left-hand of Figure 1.5.

Furthermore, such model has been extended for any arbitrary directions of ω and \mathbf{V} by means of

$$\mathbf{F}_M \approx \frac{1}{2} \rho A C_M \sin \phi V^2 \hat{\mathbf{u}} \quad (1.7)$$

where direction of \mathbf{F}_M is given by the unit vector $\hat{\mathbf{u}} = \frac{\boldsymbol{\omega} \times \mathbf{V}}{|\boldsymbol{\omega} \times \mathbf{V}|}$, and $\sin \phi$ is introduced by considering ω -component perpendicular to \mathbf{V} is the effective component of \mathbf{F}_M , and that it varies smoothly for angles $0^\circ \leq \phi \leq 90^\circ$ between ω and \mathbf{V} [6, 16].

Other Forces

Aerodynamics of rotating baseballs is computed with diverse forces like the lift and lateral forces caused by the ball seams, and the friction force acting on the spin of the ball, however, there are only few studies about these forces, which suggest such forces can be omitted. For one hand, the existing information about lift and lateral forces in balls with high spinning is that they decrease in magnitude, i.e., seams don't play an important role, besides the quick variation from positive to negative throughout the trajectory, which average their effect [7, 18, 19]. On the other hand, some studies indicate that torque forces don't affect the angular frequency or the spin axis of the ball [11, 20].

Moreover, there are temporary phenomena that could modify the trajectory of the ball like wind, rain, sudden changes in the air density, among others. However, as we have mentioned before they are strange phenomena, therefore, the majority of works don't consider them [1, 6]. Strain forces inside the ball are commonly omitted because it's clear that the ball does not suffer any deformation when it is thrown.

1.3 Concerning Knuckleballs

For many years, pitchers experiences were the main via of information about knuckleball trajectories. Speed changes, unusual movements, diverse final positions of the ball with apparent similar initial conditions and only a few studies about this phenomenon, led to think someones that the knuckleball motion was a random process [21, 22].

Nevertheless, smoothness of lift force has been studied since the 70's, when Watts & Sawyer [23] found in their wind tunnel experiments the influence of the lift force on magnitude was proportional to the square of the ball speed (similarly to others aerodynamic forces).

In addition, their measurements indicate that such force is an oscillatory force in dependence on the angle θ relative to wind direction (see Figure 1.2) in an approximate $\sin(4\theta - \pi)$ for a 4S orientation. On this regard, Borg & Morrissey [7] obtained measurements of the lift force for real pitches with 4S and 2S ball orientations (right-hand of Figure 1.5) which indicate a similar behavior to those of Watts & Sawyer [23].

The results of both works suggest the consideration of a coefficient C_{L_f} that fits the sinusoidal difference of pressure produced by the ball seams at each angle θ and ball orientation, thus computing the lift force.

In spite of all of these studies, it was not until this decade when a first model introducing the lift force in the movement equations was computed (Nathan [22]). The model is based on observations of Watts & Sawyer [23] about magnitude of lift force in dependence on the ball velocity, and it's written as

$$m\dot{\mathbf{V}} = -kC_dV^2\hat{\mathbf{V}} + kC_{L_f}V^2(\hat{\boldsymbol{\alpha}} \times \hat{\mathbf{V}}) + \mathbf{g} \quad (1.8)$$

where the first term on the right side corresponds to the drag force, the second term to the lift force, and C_d and C_{L_f} are their respective adaptive coefficients of area. Gravitational force is represented by \mathbf{g} , k is a numerical factor involving the air density ρ and the transverse sectional area A of the ball with mass m (as in equations (1.4) and (1.7)), and $\boldsymbol{\alpha}$ is a vector perpendicular to both lift force and velocity that determines the orientation of the ball. However, model (1.8) does not represent the true effect of lift force, since its sinusoidal nature is not considered in the lift coefficient C_{L_f} [22].

As a final comment, motion of non rotating baseballs and balls rotating at low angular velocities is briefly explained in Cross R. website [19]. There, Cross explains, among other things, how the lift force magnitude decrease when angular frequency increase.

1.4 Reconstruction of Trajectories: Background

Works on reconstruction of trajectories are mainly focused on either the replay of pitches on broadcasts of baseball games [24–29] or the computing of trajectories for video games [30]. Maybe this is why existing methods to do this are only focused on tracking the ball, and put aside the search of the initial conditions of the throw. Indeed, most works on tracking trajectories use all available image processing tools to fill the trajectory using the movement equations of the ball to justify their results. However, the majority of these methodologies have been reported as feasible and to have good results, in spite of physical-mathematical models are not used to reach the goal.

In more detail, the majority of tracking baseball methods consist of three parts. First, an overlap of a lot of photos of the same pitch is carried out to obtain the position of the ball at different times; also it is used to transform the 3D reality into a 2D image. Then, several trajectories are proposed in some ways such as probabilistic methods [24], database comparisons [25], and/or color and region filtering based on pixel analyses [26–28]. In this part, some discrete trajectories are filled with the same methods or by parameter estimation [29]. At last, chosen trajectories are generally compared with mathematical models.

Although, the above mentioned works are not the only reported methods to track a baseball. Studies of passive optical approach have been carried out by Theobalt et.al. [16] in order to capture the high-speed motion of baseballs. They use multiexposure images with still cameras and a stroboscope to obtain a more complete study, however, the method is poorly viable for its use.

As a reminder, our research is based on the use of the movement equations (to reconstruct trajectories) so the methodology we will show is completely different to those mentioned in this Section.

Chapter 2

Calculation of the Magnus Effect on Spinning Pitches

Purpose of this chapter is to measure the deflection of the ball caused by Magnus force at the end of its trajectory, for all possible initial conditions. In order to calculate those deflections (Section 2.3), we begin by computing the movement equations in Section 2.1 and simulating some trajectories of pitches in Section 2.2.

2.1 Equations of Motion

Accord to most of the works on spinning throws [1, 16, 31], and assumptions mentioned at the end of Section 1.2, the dynamics of a rotating baseball can be approximated by the sum of gravitational (\mathbf{F}_g), drag (\mathbf{F}_d) and Magnus (\mathbf{F}_M) forces, so that the movement equations of the baseball center of mass are commonly written as

$$m\dot{\mathbf{V}} = \mathbf{F}_d + \mathbf{F}_M + \mathbf{F}_g. \quad (2.1)$$

where $\dot{\mathbf{V}}$ is the acceleration of the ball with mass m .

However, in order to be sure that model (2.1) reproduce spinning pitches close to the reality and according to the purposes of this work, we have estimated the final deflection produced by each force involved in the dynamics of a spinning throw. All forces that produced a final deflection of more than one millimeter will be used to compute the movement equations.

The forces involved affecting the pitches inside the initial conditions range mentioned in Section 1.1, their expressions, their values of acceleration (α) and the final deflections ($d\xi$) they produce can be seen on Table 2.1, assuming the ball remains flying around a time $t = 0.5$ seconds such that $d\xi = \alpha/(2t^2)$ (according to the kinematic equations of motion [2]).

Acceleration values are computed in the following way: gravitational force varies because of the equatorial bulge [18]; values of centrifugal acceleration are computed by varying colatitude angle ψ ; Coriolis values are obtained by changing V values in throws where $\mathbf{V} \perp \boldsymbol{\Omega}$ so that they are the maximum values that can produce such force. It's a similar case to Magnus acceleration, whose values are computed taking $\phi = 90^\circ$, i.e., $\boldsymbol{\omega} \perp \mathbf{V}$ and only varying values of ω ; in turn, drag acceleration considers values of initial velocity inside the limits of a professional spinning throw (those mentioned in Section 1.1).

Approximation of centrifugal - in both radial and tangential components in relation to Earth surface - and Coriolis forces are completed according to Taylor [2]. In these approximations, the Earth is taken as a sphere rotating at constant angular velocity $\boldsymbol{\Omega}$ and moving without acceleration in its translational motion, R is the radius of the Earth, ψ is the colatitude angle at which the ball is positioned, and $\hat{\mathbf{s}}$ represents the direction of the throw projected in the $x - y$ plane.

From the values of acceleration, it's evident that the main forces are those caused by drag, Magnus and gravitational effects. It is the reason why equation (2.1) is the most frequently model used to determine the dynamics of spinning pitches. However, Table 2.1 indicates that centrifugal force - in both radial and tangential components - can produce a final deviation larger than two millimeters ($\sim 6\%$ of the radius of a baseball), thus we consider that this distance is enough to introduce centrifugal force in the movement equations. This research was limited to only consider forces producing deflections bigger than 1mm: the direction of a hit ball in a model considering the centrifugal force will be very different from one that does not take this force into account. However, the movement of the ball will match regardless of the Coriolis force.

On the other hand, as is mentioned in Sections 1.2 and 1.3, cross forces (lift and lateral) are poorly understood for spinning throws and consequently, it's difficult to estimate the maximum deflection produced by them. Nevertheless, according to Cross web site [19] and Borg & Morrissey [7], they are periodic forces (see right-hand of Figure 1.5) whose average is close to zero when the ball spins quickly, besides that their magnitude decreases when angular velocity increase. This lead us to omit cross forces from the present study.

TABLE 2.1: Estimation of acceleration (α) and deflection ($d\xi$) of a baseball caused by forces acting on a professional spinning throw.

Force	Approximation	α (cm/s ²)	$d\xi$ (cm)
Gravitational	$m\mathbf{g}$	978 - 980	~ 122
Centrifugal (rad)	$m\Omega^2 R \sin^2 \psi \hat{\mathbf{g}}$	0 - 3.4	0 - 0.42
Centrifugal (tan)	$m\Omega^2 R \sin \psi \cos \psi \hat{\mathbf{s}}$	0 - 1.7	0 - 0.21
Coriolis	$2m\mathbf{V} \times \boldsymbol{\Omega}$	0.4 - 0.7	0.05 - 0.09
Drag	$kC_d V^2 \hat{\mathbf{V}}$	650 - 1350	80 - 170
Magnus	$kC_M \sin \phi V^2 \hat{\mathbf{u}}$	140 - 850	18 - 105
Lift and/or Lateral	$kC_{Ll} V^2 \hat{\boldsymbol{\alpha}} \times \hat{\mathbf{V}}$	-	-

This is also true for torque forces. It's obvious that the baseball has a deceleration on its angular frequency ω and also experiment changes on its spin axis $\hat{\boldsymbol{\omega}}$, however, Ranger [20] predicts that rotation rate of a curveball thrown with a speed of 31 m/s and rotating at 1800 rpm decrease only by 0.08%. Moreover, experiments of Daish [11] indicate that on a golf ball more than 80% of the spin still remains after a flight of 5 seconds.

With all of this in mind, we consider the motion of a baseball is defined by

$$m\dot{\mathbf{V}} = \mathbf{F}_d + \mathbf{F}_M + \mathbf{F}_g + \mathbf{F}_{cf}, \quad (2.2)$$

so that the angular velocity $\boldsymbol{\omega}$ of the ball doesn't change neither in magnitude ω nor in spin axis $\hat{\boldsymbol{\omega}}$.

Now, substituting approximations of each force on the right side of equation (2.2), it becomes

$$m\dot{\mathbf{V}} = kC_d V^2 (-\hat{\mathbf{V}}) + kC_M \frac{V}{\omega} \boldsymbol{\omega} \times \mathbf{V} + m\mathbf{g} + m\Omega^2 R \sin^2 \psi \hat{\mathbf{g}} + m\Omega^2 R \sin \psi \cos \psi \hat{\mathbf{s}} \quad (2.3)$$

$$= kV \left[-C_d \mathbf{V} + \frac{C_M}{\omega} \boldsymbol{\omega} \times \mathbf{V} \right] + m \left[\mathbf{g} + \Omega^2 R \sin \psi (\sin \psi \hat{\mathbf{g}} + \cos \psi \hat{\mathbf{s}}) \right], \quad (2.4)$$

where $k = \frac{1}{2}\rho A$, drag C_d and Magnus C_M coefficients are functions of velocity \mathbf{V} and angular velocity $\boldsymbol{\omega}$, respectively, as shown on the left-hand side of Figure 1.5.

Thus, developing the cross product of the Magnus force term in (2.4) and defining γ as the angle between a vector pointing West and the direction of y -axis, equations of motion into components are written as

$$\begin{aligned}
\dot{V}_x &= \frac{k}{m} V \left[\frac{C_M}{\omega} (\omega_y V_z - \omega_z V_y) - C_d V_x \right] + \Omega^2 R \sin \psi \cos \psi \sin \gamma \\
\dot{V}_y &= \frac{k}{m} V \left[\frac{C_M}{\omega} (\omega_z V_x - \omega_x V_z) - C_d V_y \right] + \Omega^2 R \sin \psi \cos \psi \cos \gamma \\
\dot{V}_z &= \frac{k}{m} V \left[\frac{C_M}{\omega} (\omega_x V_y - \omega_y V_x) - C_d V_z \right] + \Omega^2 R \sin^2 \psi - g.
\end{aligned} \tag{2.5}$$

where $g \equiv |\mathbf{g}|$ is a function of ψ because of the equatorial bulge [18].

2.2 Simulation of Throws

The equation (2.5) is a coupled system of three first order nonlinear equations. This is way an analytic solution is difficult to obtain and, therefore, simulating pitches. However, it can be solved via numerically. In order to guarantee the convergence of solutions, Runge-Kutta four order method (RK4) has been employed [32].

To compute this model, the drag coefficient estimation of Adair [1] was fitted by a Boltzmann function using reduced chi-squared statistic and simplex method in OriginPro 8 program. The obtained expression is

$$C_d(V) = 0.29 + 0.22 \left[1 + e^{(V-32.37)/5.2} \right]^{-1}, \tag{2.6}$$

which is plotted on the left-hand side of Figure 1.5 by the blue sigmoidal curve. Estimation (2.6) gave a root-mean-square error under 7×10^{-3} for all values of V .

Figure 2.1 shows the trajectory for balls thrown with different initial values of \mathbf{V} and $\boldsymbol{\omega}$ at normal air density conditions (1.22 kg/m^3), colatitude of 90° , gravity of 9.8 m/s^2 , and considering the ball has a mass of 142 g and a diameter of 7.16 cm (according to the *Official Baseball Rules* [9]), whereas the distance between home and pitcher's plate is 17.05 m (see Figure 1.1). Left-hand of Figure 2.1 shows the plan view of a ball pitched in direction to home with a speed of $V = 40 \text{ m/s}$, i.e. $\mathbf{V} = (0, 40, 0) \text{ m/s}$. As seen, z -component of $\boldsymbol{\omega}$ causes the largest x -axis deflections (more than 30 cm for $|\omega_z| = 250 \text{ rad/s}$), y -component causes deflections of only a few millimeters, while a straight line is generated by the x -component.

In turn, right-hand side of Figure 2.1 shows the sectional view of a throw with initial velocity $\mathbf{V} = (0, 45, 0) \text{ m/s}$. In contrast to x -axis, ω_x is the main responsible of deflection in z -axis, while the effects of both y and z components on the trajectory are virtually non-existent.

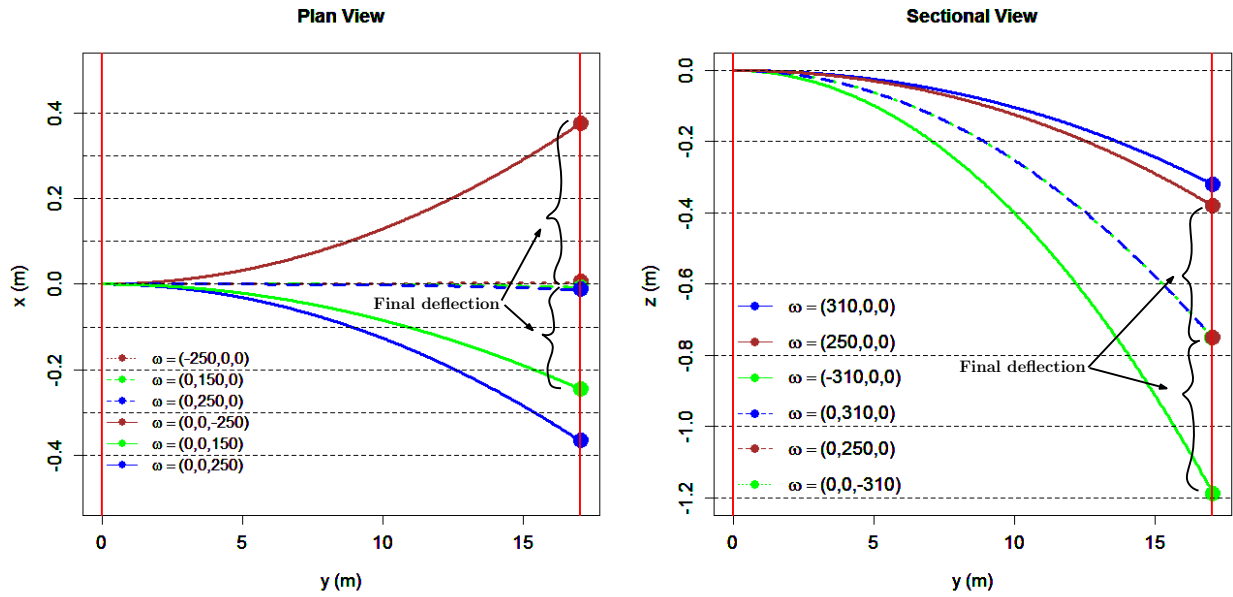


FIGURE 2.1: Ball trajectories, simulated by solving model (2.5). Left: A pitch deflects in x -axis with velocity $\mathbf{V} = (0, 35, 0)$ at different spins - in direction and magnitude -. Right: Final deflection in z axis of diverse throws with the same initial velocity $\mathbf{V} = (0, 40, 0)$ but different spin.

2.3 Final Deflection as Function of the Angular Velocity Components

With the aim of learning more about the effect of each angular velocity component, final deflection has been calculated for all possible throws in mound-home direction with initial conditions inside the limits of professional pitches. Ball, Earth and medium parameters are those used in simulations of Section 2.2.

Figure 2.2 shows the deflection at home plate produced by each component of angular velocity ω for pitches with different initial velocities $\mathbf{V} = (0, V_y, 0)$, $V_y \in [30, 50]$ m/s. Deflections are calculated by subtracting final positions from those obtained from solving system (2.5) without Magnus force terms, also via RK4. Deflections in the same direction of angular velocity components aren't plotted because they are zero for all values by construction of the model [6], e.g., Magnus acceleration is zero on the first equation of system (2.5) when angular velocity takes values distinct to zero only in x -component, such that $\omega = (\omega_x, 0, 0)$.

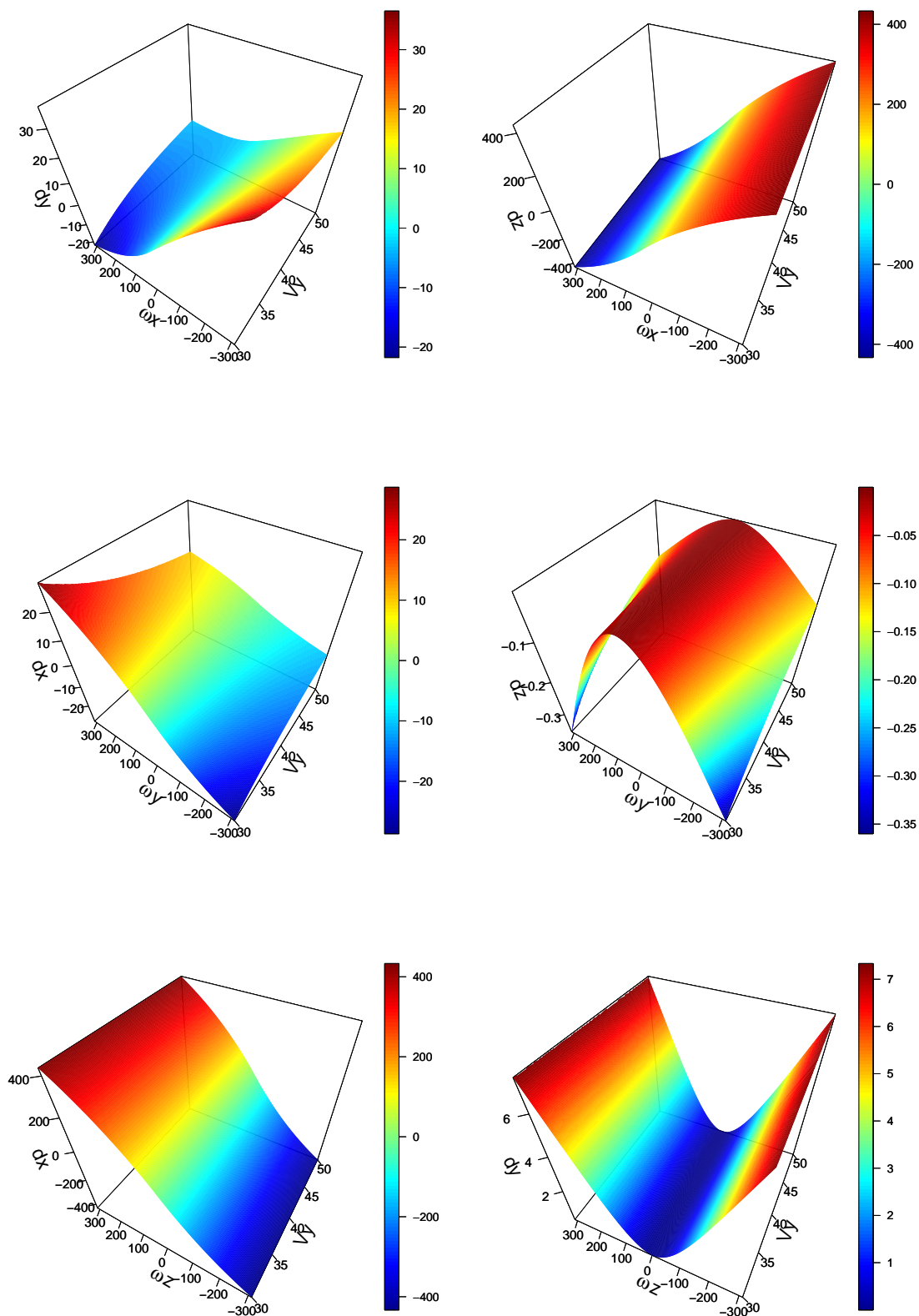


FIGURE 2.2: Final deflection in function of velocity and angular velocity for balls thrown with $\mathbf{V} = (0, V_y, 0)$, $V_y \in [30, 50]$ m/s. Up: Spin of $\boldsymbol{\omega} = (\omega_x, 0, 0)$. Center: Spin of $\boldsymbol{\omega} = (0, \omega_y, 0)$. Down: Spin of $\boldsymbol{\omega} = (0, 0, \omega_z)$; $\omega_x, \omega_y, \omega_z \in [-310, 310]$ rad/s.

In the graphics, the importance of the system of axes defined in Section 1.1 concerning the relations between \mathbf{V} and $\boldsymbol{\omega}$ components in system (2.5) can be seen. Values of ω_z produce larger deflections in x -axis (dx) than those caused by ω_y in a proportion of $dx_{\omega_z} \sim 10dx_{\omega_y}$. This is because ω_z is related to V_y , which takes the largest values of all velocity components. A similar case occurs at z -axis where ω_x is connected to V_y .

On the other hand, deflections in y -axis allow us to observe the role of V_z on throws: maximum deflections produced by ω_x are slightly larger than those one by ω_z because graphics are computed with initial V_z equal to zero, therefore it reaches higher values than V_x by gravitational force. However, difference between deflections would be lower or higher for the cases in which V_z takes positive or negative initial values, respectively.

Moreover, this is connected to the inverse shape of up-left and center-left meshes in Figure 2.2, whose angular velocity terms are related to V_z in system (2.5); in turn, up-right and bottom-left graphics are similar in relation to V_y , whereas center-right and bottom-right show the same behavior to V_x .

Thus, for common pitches with V_z close to zero, deflection in x -axis is mainly caused by ω_z and in a lesser extent by ω_y , while deflections in y and z axes are practically caused by ω_x . This means that if the purpose of this work was changed to simulate pitches with precision of 10^{-2} m, system (2.5) could be rewritten as

$$\begin{aligned}\dot{V}_x &= \frac{k}{m}V \left[\frac{C_M}{\omega} (\omega_y V_z - \omega_z V_y) - C_d V_x \right] \\ \dot{V}_y &= \frac{k}{m}V \left[-\frac{C_M}{\omega} (\omega_x V_z) - C_d V_y \right] \\ \dot{V}_z &= \frac{k}{m}V \left[\frac{C_M}{\omega} (\omega_x V_y) - C_d V_z \right] - g,\end{aligned}\tag{2.7}$$

where centrifugal force is also omitted. However, we keep the initial purpose of this work and leave model (2.7) as an alternative for studies with different objectives.

Chapter 3

Reconstruction of Trajectories

3.1 Energetic Analysis of the Movement Equations

First we notice that equation (2.3) can be rewritten as

$$\frac{d\mathbf{V}}{dt} = \alpha V\mathbf{V} + V(\boldsymbol{\beta} \times \mathbf{V}) + \boldsymbol{\Gamma} \quad (3.1)$$

where $\alpha = -\frac{kC_D}{m}$, $\boldsymbol{\beta} = \frac{kC_M}{m\omega}\boldsymbol{\omega}$, and $\boldsymbol{\Gamma} = \frac{\mathbf{F}_g + \mathbf{F}_{cf}}{m}$. As a comparison, equation (3.1) is the analogous of the Lorentz equation of a charged particle in electromagnetism theory [33], so that the first term (drag force) is the equivalent of the electric field, while the second one (Magnus force) is related to the magnetic field.

The Equation of Work

Developing the scalar product between equation (3.1) and \mathbf{V} ,

$$\begin{aligned} \frac{d\mathbf{V}}{dt} \cdot \mathbf{V} &= (\alpha V\mathbf{V} + V(\boldsymbol{\beta} \times \mathbf{V}) + \boldsymbol{\Gamma}) \cdot \mathbf{V} \\ &= \alpha V\mathbf{V} \cdot \mathbf{V} + V(\boldsymbol{\beta} \times \mathbf{V}) \cdot \mathbf{V} + \boldsymbol{\Gamma} \cdot \mathbf{V}. \end{aligned} \quad (3.2)$$

Then, equation (3.2) can be simplified to

$$\frac{d}{dt} \left(\frac{V^2}{2} \right) = \alpha V^3 + \boldsymbol{\Gamma} \cdot \mathbf{V} \quad (3.3)$$

by definition of scalar product and orthogonality of vector product.

Equation (3.3) indicates that angular velocity - involved in $\boldsymbol{\beta}$ - only changes the direction of the ball but it doesn't play a role in the work carried out by the system, like the action of the magnetic field on a charged particle [33]. Such result will be very important in order to support the trajectories reconstruction method on the following Section 3.3.

Now, with the purpose of having a comparison method of solution to main one of Section 3.2, equation (3.3) is discretized to obtain the discrete scheme

$$\frac{\Delta \mathbf{V}_j}{\Delta t_j} \cdot \mathbf{V}_j = \alpha_j V_j^3 + \boldsymbol{\Gamma} \cdot \mathbf{V}_j \quad (3.4)$$

where velocity \mathbf{V}_j and acceleration $\Delta \mathbf{V}_j / \Delta t_j$ of the ball are known at n times t_j , $j = 1, \dots, n$, and α_j varies in time because it is in function of magnitude of velocity V_j . Thus, a recursive algorithm can be computed by knowing the values of \mathbf{V}_1 , \mathbf{V}_2 , $\Delta \mathbf{V}_1 / \Delta t_1$ in equation (3.4), and obtaining a similar discrete expression to the angular velocity, which is carried out below.

As a comment, equation (3.4) could be modified having in mind a parameter estimation, so that

$$\alpha_j = \frac{1}{V_j^3} \left[\frac{\Delta \mathbf{V}_j}{\Delta t} \cdot \mathbf{V}_j - \boldsymbol{\gamma} \cdot \mathbf{V}_j \right],$$

however, such equation is not used in the present research.

The Effective Angular Velocity

The effective angular velocity of a pitch can be calculated by the vector product $\mathbf{V} \times$ (3.1), such that

$$\begin{aligned} \mathbf{V} \times \frac{d\mathbf{V}}{dt} &= \mathbf{V} \times (\alpha V \mathbf{V} + V(\boldsymbol{\beta} \times \mathbf{V}) + \boldsymbol{\Gamma}) \\ &= \alpha V (\mathbf{V} \times \mathbf{V}) + \mathbf{V} \times V(\boldsymbol{\beta} \times \mathbf{V}) + \mathbf{V} \times \boldsymbol{\Gamma} \\ &= V [\mathbf{V} \times (\boldsymbol{\beta} \times \mathbf{V})] + \mathbf{V} \times \boldsymbol{\Gamma}, \end{aligned}$$

since $\mathbf{V} \times \mathbf{V} = 0$. Then, using the triple product expansion,

$$\begin{aligned} \mathbf{V} \times \frac{d\mathbf{V}}{dt} &= V [\boldsymbol{\beta}(\mathbf{V} \cdot \mathbf{V}) - \mathbf{V}(\mathbf{V} \cdot \boldsymbol{\beta})] + \mathbf{V} \times \boldsymbol{\Gamma} \\ &= V [\boldsymbol{\beta} V^2 - \mathbf{V}(\mathbf{V} \cdot \boldsymbol{\beta})] + \mathbf{V} \times \boldsymbol{\Gamma} \\ &= V^3 \left[\boldsymbol{\beta} - \frac{\mathbf{V}(\mathbf{V} \cdot \boldsymbol{\beta})}{V^2} \right] + \mathbf{V} \times \boldsymbol{\Gamma}, \end{aligned} \quad (3.5)$$

where it can be noted that $\boldsymbol{\beta}' = \boldsymbol{\beta} - \mathbf{V}(\mathbf{V} \cdot \boldsymbol{\beta}) / V^2$ is the effective component of $\boldsymbol{\beta}$ since by the meaning of the scalar product

$$\begin{aligned}\frac{\mathbf{V}(\mathbf{V} \cdot \boldsymbol{\beta})}{V^2} &= \frac{V^2 \beta \cos \phi \hat{\mathbf{V}}}{V^2} \\ &= \beta \cos \phi \hat{\mathbf{V}}\end{aligned}\quad (3.6)$$

Thus, equation (3.6) represents the projection of vector $\boldsymbol{\beta}$ in direction of \mathbf{V} , where ϕ is the minimum angle between vectors \mathbf{V} and $\boldsymbol{\beta}$, as in model (1.7).

Therefore, when substituting and solving equation (3.5) for $\boldsymbol{\beta}'$, we have

$$\begin{aligned}\boldsymbol{\beta}' &= \frac{1}{V^3} \left[\mathbf{V} \times \frac{d\mathbf{V}}{dt} - \mathbf{V} \times \boldsymbol{\Gamma} \right] \\ &= \frac{\mathbf{V}}{V^3} \times \left[\frac{d\mathbf{V}}{dt} - \boldsymbol{\Gamma} \right].\end{aligned}\quad (3.7)$$

Similarly to scheme (3.5), equation (3.7) can be discretized as

$$\boldsymbol{\beta}'_j = \frac{\mathbf{V}_j}{V_j^3} \times \left[\frac{\Delta \mathbf{V}_j}{\Delta t_j} - \boldsymbol{\Gamma} \right] \quad (3.8)$$

which completes the recursive algorithm proposed above.

3.2 The Method for Reconstructing Trajectories

We begin this section citing Turing's work [34] on the "Imitation Game" because the reconstruction of trajectories problem must be re-defined in a similar way to that he proposes about whether a machine can think. Turing dealt with rephrasing such question to answer it.

Regarding the reconstruction of trajectories problem in the way we propose, the first question that comes to mind is: how many ball positions in function of time are necessary to reconstruct a complete trajectory? This is a little misleading because the answer should be related with both the method employed to complete them and the physics involved in a throw. However, if we focus only on the nature of a pitch, leaving aside the methodology, our original question could be replaced with "how many positions of the ball in function of time define a throw?", in other words, "how many positions of the ball in function of time are necessary to obtain the initial conditions of a throw?"

New questions are namely more related to the purposes of this thesis. We answer them with the analysis showed below, where we found the need of only knowing three points. Thus, the task of developing an algorithm that requires such number of points comes up.

Characterization of a Trajectory by 3 Points of It

As a starting point, we must thinking about movement equations (2.5) without Magnus force terms,

$$\begin{aligned}\ddot{x} &= -\frac{kC_d}{m}VV_x + \Omega^2 R \sin \psi \cos \psi \sin \gamma \\ \ddot{y} &= -\frac{kC_d}{m}VV_y + \Omega^2 R \sin \psi \cos \psi \cos \gamma \\ \ddot{z} &= -\frac{kC_d}{m}VV_z + \Omega^2 R \sin^2 \psi - g,\end{aligned}\tag{3.9}$$

where $\ddot{x} \equiv \dot{V}_x$, $\ddot{y} \equiv \dot{V}_y$, $\ddot{z} \equiv \dot{V}_z$ are the accelerations of the ball in x , y and z components, respectively.

Resulting system (3.9) is significantly less complicated, but it's still difficult to solve its initial value problem (simulating pitches) by traditional analytic methods¹ [35, 37] and even more for its boundary value problem (reconstruction of trajectories) [37–39]. However, there are numerical researches about this kind of problems. Their results are captured in some theorems demonstrated via numerical methods [38], like Theorem 3.1, which we use to support the methodology assumptions.

Theorem 3.1. [32, 38]

Assuming that function f in the boundary value problem (BVP)

$$y'' = f(t, y, y'), \quad \text{for } t_1 \leq t \leq t_2, \quad \text{with } y(t_1) = y_1 \text{ and } y(t_2) = y_2,\tag{3.10}$$

is continuous in the set

$$D = (t, y, y') \mid \text{for } t_1 \leq t \leq t_2, \quad \text{with } -\infty \leq y \leq \infty \text{ and } -\infty \leq y' \leq \infty,\tag{3.11}$$

and that partial derivatives f_y and $f_{y'}$ are also continuous in D . If

- (i) $f_y(t, y, y') > 0$, for all $(t, y, y') \in D$ and
- (ii) there exist a constant M such that

$$|f_{y'}(t, y, y')| \leq M, \quad \text{for all } (t, y, y') \in D,\tag{3.12}$$

then the BVP has an unique solution.

¹We have only found a research (Sayed [36]) in which a similar system to (3.9) is solved analytically.

Now, we want to reconstruct the trajectory by solving the boundary value problem (BVP) for system (3.9) assuming two points in function of time of a ball trajectory, namely $\xi_1 = \xi(t_1)$ and $\xi_3 = \xi(t_3)$, with $t_1 < t_3$, are known.

All equations of the system have the form (3.10) and (3.11), so Theorem 3.1 guarantees the uniqueness of the solution for each one, if conditions (i) and (ii) of (3.12) are satisfied. We need to prove it².

First, it can be noticed that movement equations (3.9) don't depend on the ball position ξ , i.e, $\ddot{\xi} = f(t, \dot{\xi})$, therefore condition (i) doesn't need be satisfied because it's a trivial case, although $f_{\xi} = 0$ for all $(t, \dot{\xi}) \in D$. Regarding condition (ii), it's clear $f_{\mathbf{v}}$ is bounded for all $(t, \dot{\xi}) \in D$ since all C_d , V , V_x and their derivatives are always bounded. Therefore constant M exist, and thus the two-point BVP for the equations of motion without Magnus force has an unique solution, i.e, ball trajectories computed with this model can be characterized by two of their points.

This shouldn't be surprising if we analyze it from the physics point of view of a typical ballistic throw: a projectile thrown from point ξ_1 at time t_1 that goes over a second point ξ_3 at t_3 . It's not difficult to think there is only one initial velocity (V_x, V_y, V_z) that can produce the ball pass at positions (x_2, y_2, z_2) , (x_3, y_3, z_3) in time t_2 and t_3 , respectively³.

But, what if the Magnus force is introduced in system (3.9)? By equation (3.3), we know the Magnus force only changes the trajectory of the ball but it's not involved in the work carried out (this result permitted us to omit such force momentarily at the beginning of this Section). Furthermore, graphics of Figure 2.2 indicate those changes (deflection of the ball) are not oscillatory for $|\omega|$, in effect, final deflections components are monotonically increasing (or decreasing). This motivates to think only another point ξ_2 , with $t_1 < t_2 < t_3$, is necessary to represent a complete trajectory.

Note: We don't intend to say that the three-points boundary-value problem for system (2.5) has a unique solution! Evidently this assumption would be wrong since the equations of system (2.5) are coupled and the same effect can be produced by different ω -components, which can be seen in Figure 2.2: Final deflections remain increasing (or decreasing) for $|\omega|$, but it's not the same case for ω in all meshes. However, we suggest that one solution of the problem can be found.

²We don't develop a rigorous proof since there are other ways to prove only two-points are necessary to solve the BVP for model (3.9), like the physical analysis shown above.

³Indeed, there could be a small interval of possible initial conditions due to the behavior of drag coefficient, however, it would be very small since speed of the projectile doesn't changes significantly.

The Method

Based on this proposal, initial conditions of any trajectory can be obtained by minimizing the function

$$f(\mathbf{V}, \boldsymbol{\omega}) = \sum_{i=1}^3 \|\boldsymbol{\xi}_i - \mathbf{p}_i\|, \quad (3.13)$$

where $\mathbf{p}_i \equiv \mathbf{p}_i(t_i)$ are the ball positions at time t_i of a possible trajectory, and $\|\cdot\|$ refers to the euclidean distance. Moreover, position of the ball at point $\boldsymbol{\xi}_1$ is known, since is the origin of the trajectory, thus equation (3.13) could be simplified to

$$f(\mathbf{V}, \boldsymbol{\omega}) = \sum_{i=2}^3 \|\boldsymbol{\xi}_i - \mathbf{p}_i\|. \quad (3.14)$$

Now, the question is how to minimize it. To answer this, we may point out that a more accurate estimation of the velocity can be made at the beginnings of a throw because the largest deflections occasioned by Magnus force occur at the end of the trajectory (and then the dynamics of the ball at the points closest to the initial point is practically determined by its initial velocity). Thus, minimization of distance $\|\boldsymbol{\xi}_2 - \mathbf{p}_2\|$ in function (3.14) shall be related with finding values of initial velocity, whereas the angular velocity shall be connected to $\|\boldsymbol{\xi}_3 - \mathbf{p}_3\|$.

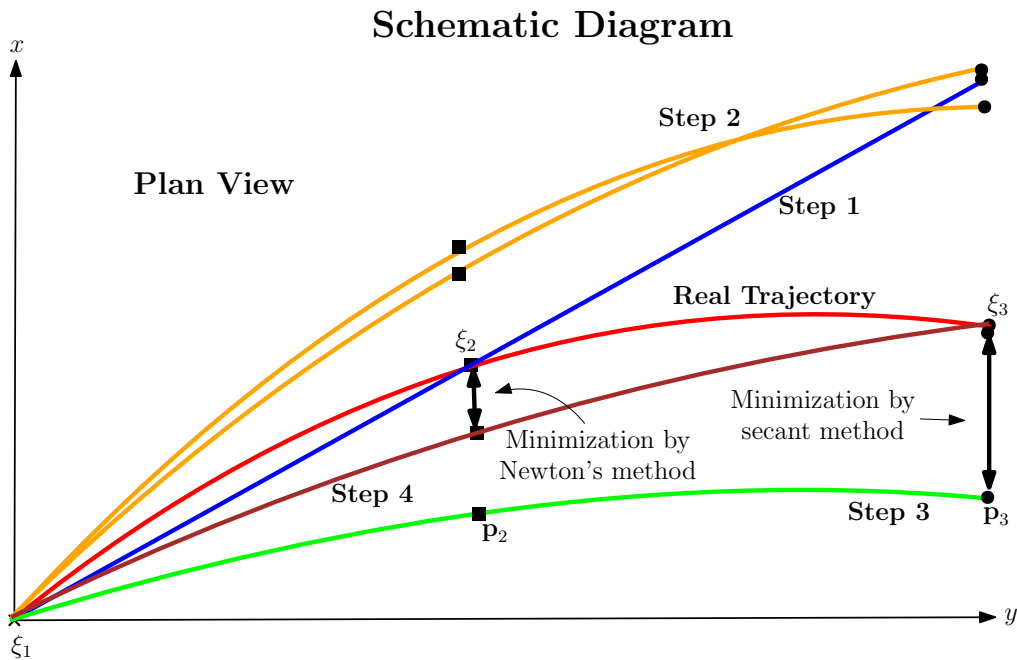
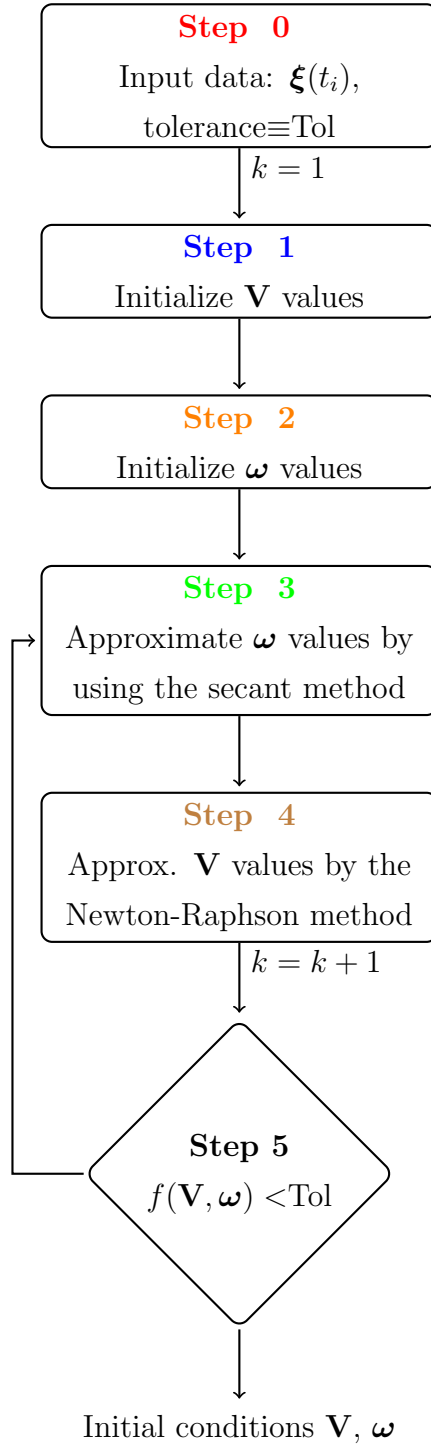


FIGURE 3.1: Schematic diagram of the algorithm. Newton-Raphson method is responsible for minimizing the distance between data \mathbf{p}_2 and proposed point $\boldsymbol{\xi}_2$ by approximating \mathbf{V} , while secant method does the same for points at time t_3 by approximating $\boldsymbol{\omega}$. Colors are according to steps in Algorithm 3.1.

Algorithm 3.1.**Newton-Raphson Method**

$$\mathbf{V}^k = \mathbf{V}^{k-1} - \frac{\mathbf{p}(t_2, \mathbf{V}^{k-1}) - \xi_2}{\frac{d\mathbf{p}}{d\mathbf{V}}(t_2, \mathbf{V}^{k-1})}$$

Secant Method

$$\omega_x^k = \omega_x^{k-1} - \frac{(z(t_3, \omega_x^{k-1}) - z_3)(\omega_x^{k-1} - \omega_x^{k-2})}{(z(t_3, \omega_x^{k-1}) - z_3) - (z(t_3, \omega_x^{k-2}) - z_3)},$$

$$\omega_y^k = \omega_y^{k-1} - \frac{(x(t_3, \omega_y^{k-1}) - x_3)(\omega_y^{k-1} - \omega_y^{k-2})}{(x(t_3, \omega_y^{k-1}) - x_3) - (x(t_3, \omega_y^{k-2}) - x_3)},$$

$$\omega_z^k = \omega_z^{k-1} - \frac{(x(t_3, \omega_z^{k-1}) - x_3)(\omega_z^{k-1} - \omega_z^{k-2})}{(x(t_3, \omega_z^{k-1}) - x_3) - (x(t_3, \omega_z^{k-2}) - x_3)}$$

Such observation along with the commonly use of the shooting method to solve two-point BVP of equations similar to (3.9), using Newton-Raphson method to obtain a solution for the initial value problem (IVP) [32], leads to construct a method consisting of two interrelated parts (or objectives), as it's described in Algorithm 3.1 and either in Figure 3.1.

The algorithm consist of five steps:

- **Step 0.** Data points and parameters of the method are defined.
- **Step 1.** Shooting method is applied to obtain the first velocity approximation \mathbf{V}^0 , using points ξ_1 and ξ_2 , considering the assumptions mentioned in this Section. Additionally, such assumptions permit us to use Newton-Raphson method to solve the IVP.
- **Step 2.** Initial values for angular velocity are defined. We suggest $\omega^0 = (-50, -50, -50)$ rad/s and $\omega^1 = (50, 50, 50)$ rad/s (hoping to have initial approximations covering the search space but inside the range of possible solutions).
- **Step 3.** The wide range of angular velocity solutions demands to solve the IVP by a slower method in convergence than Newton-Raphson, this leads us to use the secant method, where ω^k – components are approximated according to the results of Section 2.3, with the restriction $|\omega^k| < 310$ rad/s to keep the solutions inside the search space.
- **Step 4.** New velocity \mathbf{V}^k values are obtained in a similar way to that of Step 2 but considering the obtained ω^k values.
- **Step 5.** Steps 3 and 4 are repeated as in an iterative way until minimizing function (3.14) below the tolerance (Tol) defined in Step 0.

3.3 Results

The Algorithm 3.1 is applied to some synthetic trajectories, which are generated by solving (2.5) as in Section 2.2 and with the same parameters.

Table 3.1 shows the results for the reconstruction of a ball thrown at time $t_0 = 0$ from the origin $\xi_1 = (0, 0, 0)$, which reaches home at position $\xi_3 = (2.6 \times 10^{-3}, 17.05, -3.3 \times 10^{-1})$ measuring in meters, at time $t_3 = 0.388$, and varying data ξ_2 . The stop rule consist on minimizing the function (3.14) below tolerance Tol= 10^{-4} m. The test corresponds to the pitch with initial conditions $\mathbf{V} = (0, 45, 0)$ m/s, $\omega = (300, 0, 0)$ rad/s. To complement it, the distance between the obtained and the real trajectories throughout the flight of the ball is plotted in Figure 3.2.

As can be seen on the same Figure, better solutions for such study are reached when used y_2 approximates to y_1 . This is because of the construction of the method: choosing a value of ξ_2 close to the initial point ξ_1 allow us to obtain a better approximation of \mathbf{V} in Step 1

of Algorithm 3.1; in turn, a good first approximation of the ball velocity is very important since it permit us to focus all the iterations to approximate $\boldsymbol{\omega}$ and only improving \mathbf{V} values. In this way, better (regarding function f) and faster (low number of iterations) solutions are obtained from the methodology of Newton-Raphson (\mathbf{V}) and secant methods ($\boldsymbol{\omega}$) [32, 43].

TABLE 3.1: Four trajectories are obtained by using method described in Algorithm 3.1, varying the location of the ball position $\boldsymbol{\xi}_2$, e.g., the results in black are those obtained by locating y_2 at three-quarter parts of distance between y_3 and y_1 . Initial velocity \mathbf{V} and angular velocity $\boldsymbol{\omega}$ are obtained by minimizing the function $f(\mathbf{V}, \boldsymbol{\omega})$ in a k number of iterations. In addition, the obtained initial conditions by energetic-method are shown as well.

Parameters	Results				
	$\boldsymbol{\xi}_2$ location	\mathbf{V} (m/s)	$\boldsymbol{\omega}$ (rad/s)	$f(\mathbf{V}, \boldsymbol{\omega})$	k iter.
$\frac{3}{4}(y_3 - y_1)$		$(-1.8 \times 10^{-3}, 45.00, 1.2 \times 10^{-3})$	$(300.8, 39.9, -2.8)$	8.4×10^{-5}	27
$\frac{1}{2}(y_3 - y_1)$		$(-1.2 \times 10^{-3}, 45.00, 6.1 \times 10^{-4})$	$(301.0, 39.8, -2.7)$	6.4×10^{-5}	13
$\frac{1}{3}(y_3 - y_1)$		$(-7.9 \times 10^{-4}, 45.00, 5.7 \times 10^{-4})$	$(301.1, 39.8, -2.6)$	5.1×10^{-5}	9
$\frac{1}{4}(y_3 - y_1)$		$(-5.9 \times 10^{-4}, 45.00, 3.3 \times 10^{-4})$	$(301.1, 39.7, -2.5)$	2.5×10^{-5}	8
Energetic method		$(5.1 \times 10^{-5}, 44.98, -5.9 \times 10^{-3})$	$(224.0, 0.61, -2.6)$	80	-
Initial Values:		$(0, 45, 0)$	$(300, 0, 0)$		

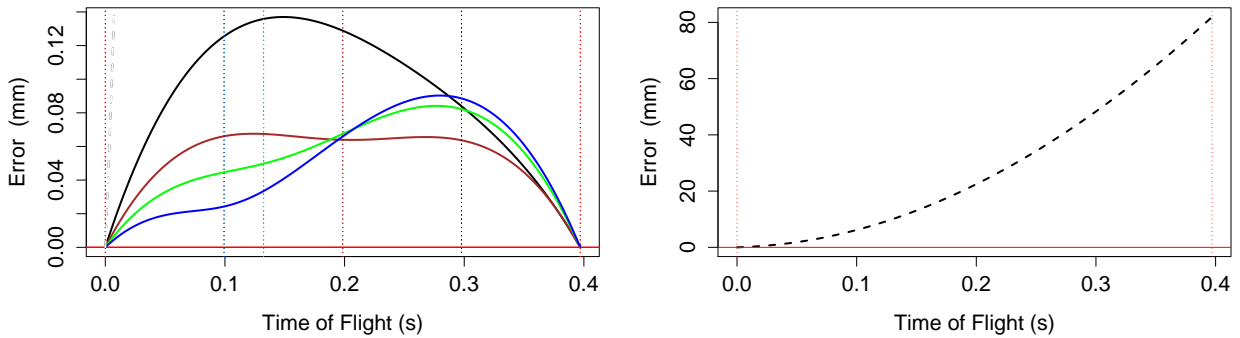


FIGURE 3.2: Error between trajectories along the pitch. Left: Using the method proposed in Algorithm 3.1. Right: Using the method proposed in Section 3.1. Colors are according to data in in Table 3.1. Red vertical dashed lines tag the times t_1 and t_3 whereas other colors tag times when the ball cross y_2 .

However, for all positions of $\boldsymbol{\xi}_2$, the obtained trajectories are always close to the real one ($\text{err} < 0.2$ mm), although the error is not constant. This occurs because the method is designed to search the values that minimize the distance at the intermediate time (tag with dashed-color lines in Table 3.1) and at final time (tag with red-dashed line).

The second test consist of a throw with initial conditions $\mathbf{V} = (2, 39, 1)$ m/s, $\boldsymbol{\omega} = (30, 80, 200)$ rad/s, which makes the ball cross home-plate at $\boldsymbol{\xi}_3 = (-3.1 \times 10^{-1}, 17.08, -9.6 \times 10^{-1})$, with

$t_3 = 0.461$, taking $\xi_1 = (0, 0, 0)$ as the initial position. It shows the other side of choosing a y_2 point very close to y_1 : this could produce a slight divergence of the obtained trajectory at the end of it, while trajectories with y_2 points near to the midpoint remain in convergence, see left-hand of Figure 3.3.

According to Table 3.2, the method seems to converge around with the same iterations of the first case of study. More precisely, in both cases values of \mathbf{V} are approximated with an accurate of 10^{-3} m/s for all ξ_2 points chosen.

TABLE 3.2: Results for the second test. Same notations as for Table 3.1.

Parameters	Results			
	ξ_2 location	\mathbf{V} (m/s)	$\boldsymbol{\omega}$ (rad/s)	$f(\mathbf{V}, \boldsymbol{\omega})$
$\frac{3}{4}(y_3 - y_1)$	(2.002, 39.00, 0.999)	(28.6, 49.9, 195.6)	8.8×10^{-5}	26
$\frac{1}{2}(y_3 - y_1)$	(2.001, 39.00, 0.999)	(28.9, 58.6, 195.7)	9.3×10^{-5}	13
$\frac{1}{3}(y_3 - y_1)$	(2.000, 39.00, 0.999)	(29.2, 64.2, 196.0)	9.1×10^{-5}	10
$\frac{1}{4}(y_3 - y_1)$	(2.000, 39.00, 0.999)	(29.8, 67.0, 196.1)	9.8×10^{-5}	8
Energetic method	(1.995, 38.99, 0.986)	(23.7, 15.9, 170.0)	35	-
Initial Values:	(2, 39, 1)	(30, 80, 200)		

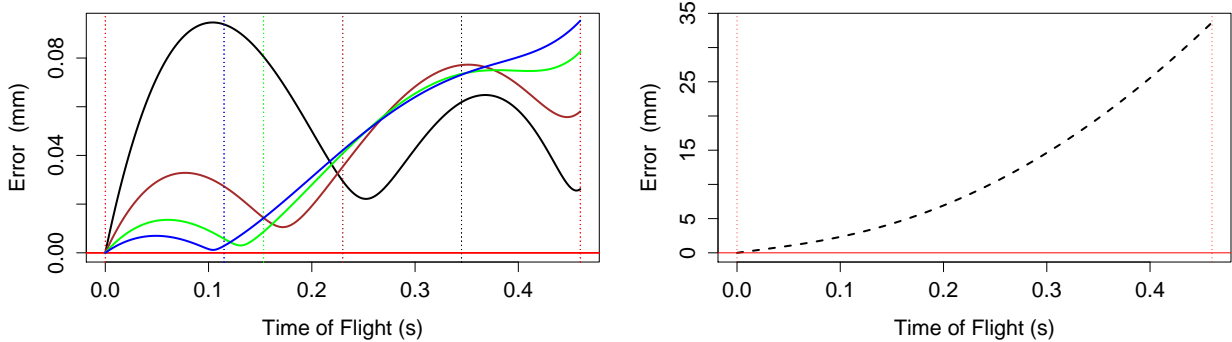


FIGURE 3.3: Error between trajectories along the pitch. Left: Using method proposed in Algorithm 3.1. Right: Using energetic method proposed in Section 3.1. Colors are according to data in Table 3.2.

Regarding $\boldsymbol{\omega}$ approximations, even though this method doesn't get solutions close that to the data, it sufficiently approximates ω_x and ω_z to fit the real trajectory; in turn, ω_y values are very far from the optimum value but it's not represented because of the role of ω_y in the meshes of Figure 2.2.

On the other hand, the method proposed in Section 3.1 is computed using all n position values of the synthetic trajectory to obtain the \mathbf{V}_j , $\Delta\mathbf{V}_j/\Delta t_j$ and β_j , $j = 1, \dots, n$ values

in an explicit scheme [43]. Approximations using this method are very far from the real initial conditions, which produce an erratic trajectory that moves away the real one in an exponential way, as shown in right of Figure 3.2. These poor results are the outcome of the strong dependence on the initial velocity we have mentioned along this work: It only requires to calculate the initial velocity once but such approximation isn't sufficiently good, and consequently the obtained angular velocity values are wrong.

Tests were carried out by using R-Statistics program in a Lenovo 400 RAM, 250 GB, Intel-Core i5 computer. Under this conditions, computing time are below 10 seconds for both study cases, even for reconstructions with high numbers of iterations.

Chapter 4

The Knuckleball

4.1 Lift Force Model for 4S and 2S Ball Orientations

As mentioned in Section 1.3, lift force can be approximated by

$$\mathbf{F}_{\text{Lf}} \approx kC_{\text{Lf}}V^2(\hat{\boldsymbol{\alpha}} \times \hat{\mathbf{V}}) \quad (4.1)$$

with the lift coefficient C_{Lf} in function of the ball seams. Specifically for 4S and 2S orientations, such coefficient should have a similar behavior to the experimental data of Borg & Morrisey shown on the right-hand side of Figure 1.5.

From Figure 1.5, it's clear that the function

$$f(\theta) = a_0 \sin(4\theta - \pi), \quad (4.2)$$

with the constant coefficient a_0 , is implied on its behavior as is hinted by Watts & Sawyer [23] and mentioned by Borg & Morrisey [7].

In this way, equation (4.2) could be considered as the first model for the lift coefficient. It coincides in period with the two ball orientations and fits better to the 4S orientation, mainly when the seams are symmetrical in up-down sides of the ball, which corresponds to the angles at which the value of the lift coefficient is zero or close to zero. However, it doesn't represent the extra-imbalance of forces occurring when the non-symmetry on the seams appears.

Then, to obtain a model that fits to the experimental data it's important to understand and complete the effect of the stitches on the lift force. The first logical assumption is to think that the aerodynamics of the ball is modified by the distances between the position of each

stitch and stagnation ball point (see Figure 1.2), so that the stitches close to the front of the ball originate a turbulent boundary layer and a difference in pressure making the ball to move in their direction, in a similar way as the wings of an airplane [40–42].

Thus, we propose a discrete scheme in which the seams are represented by a collection \mathbf{S} of n stitches with vector positions \mathbf{s}_i , $i = 1, \dots, n$. Each stitch affects the magnitude of the lift force as the sine function in equation (4.3), whereas the direction of disturbance is given by the sign function inside it. In this way, since $\mathbf{S} \equiv \mathbf{S}(\theta)$, the total effect $h(\theta)$ of seams is expressed as

$$h(\theta) = \sum_{i=1}^n \sin \left(\frac{\|\mathbf{s}_i - \mathbf{p}\|\pi}{2d} + \pi/2 \right) \cdot \text{sgn}(p^* - s_i^*) \quad (4.3)$$

where \mathbf{p} is the stagnation point for the ball with diameter d , s_i^* and p^* are the components of \mathbf{s}_i and \mathbf{p} in the axis of motion of the ball.

As seen in Figure 4.1, the scheme adjusts to the boundary conditions because stitches located exactly at the front or back of the ball don't produce an imbalance of forces, however as soon as a stitch is close to \mathbf{p} , it breaks the symmetry and a force is produced according to the fluid mechanics theory [40, 42].

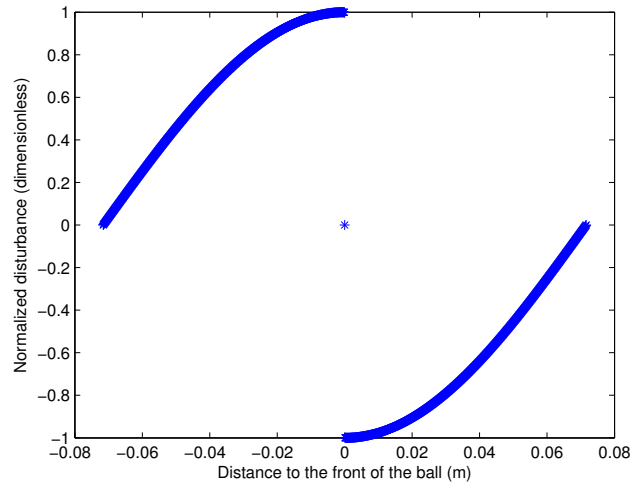


FIGURE 4.1: Effect of stitches in c_L as function of distances $\|\mathbf{s}_i - \mathbf{p}\|$. Negative distances represent negatives values of $p^* - s_i^*$.

Therefore, assuming that the forces involved in the lift of the ball act as an additive system, the lift coefficient can be completed as the sum of (4.2) and (4.3), such that

$$C_{Lf}(\theta) = a_0 \sin(4\theta - \pi) + a_1 \sum_{i=1}^n \sin \left(\frac{\|\mathbf{s}_i - \mathbf{p}\|\pi}{2d} + \pi/2 \right) \cdot \text{sgn}(p^* - s_i^*). \quad (4.4)$$

where the constant coefficient a_1 is joined to the stitches term for obtaining a weight function.

And so, according to Nathan model (4.1), the lift force acting on an upward-direction is derived by

$$\mathbf{F}_{\text{Lf}} = kC_{\text{Lf}}V^2(\hat{\boldsymbol{\beta}} \times \hat{\mathbf{V}}) \quad (4.5)$$

where C_{Lf} is taken from (4.4), and the vector $\boldsymbol{\beta}$ points outward the pictures in Figure 1.2 to obtain the lift force in upward direction¹.

4.2 Results and Knuckleball Trajectories

Values of the Lift Coefficient

A parameter estimation for a_0 and a_1 coefficients has been carried out in order to fit the equation (4.4) to the experimental data shown on the right-hand side of Figure 1.5. We have carried out it in two ways: trial and error and least-square method.

Least-square estimation conduce to minimize

$$G(a_0, a_1) = \sum_{j=1}^m \left[a_0 \kappa_j + a_1 \sum_{i=1}^n \lambda_{i,j} - d_j \right]^2, \quad (4.6)$$

taking $\kappa_j = \sin(4\theta_j - \pi)$, $\lambda_{i,j} = \sin\left(\frac{|\mathbf{s}_{i,j} - \mathbf{p}|\pi}{2d} + \pi/2\right) \cdot \text{sgn}(p^* - s_{i,j}^*)$ to compute the lift coefficient as in equation (4.4), and with d_j , $j = 1, \dots, m$, the m Borg & Morrissey data [7].

According to the least-square theory [43], the equivalent system

$$\begin{bmatrix} \sum_{j=1}^m [\kappa_j^2] & \sum_{j=1}^m [\kappa_j \sum_{i=1}^n \lambda_{i,j}] \\ \sum_{j=1}^m [\kappa_j \sum_{i=1}^n \lambda_{i,j}] & \sum_{j=1}^m [\sum_{i=1}^n (\lambda_{i,j})^2] \end{bmatrix} \begin{bmatrix} a_0 \\ a_1 \end{bmatrix} = \begin{bmatrix} \sum_{j=1}^m [d_j \kappa_j] \\ \sum_{j=1}^m [d_j \sum_{i=1}^n (\lambda_{i,j})] \end{bmatrix}, \quad (4.7)$$

is solved by obtaining $a_0 = 0.058$, $a_1 = 0.006$ for 4S orientation, and $a_0 = 0.186$, $a_1 = 0.006$ for 2S orientation.

On the other hand, trial an error method has been developed having in mind that on the equation (4.4) can be modified as the average of equation (4.2) and the average of the stitches effect , so that

$$C_{\text{Lf}}(\theta) = \frac{1}{2} \left[b_0 \sin(4\theta - \pi) + \frac{1}{n} \sum_{i=1}^n \sin\left(\frac{|\mathbf{s}_i - \mathbf{p}|\pi}{2d} + \pi/2\right) \cdot \text{sgn}(p^* - s_i^*) \right]. \quad (4.8)$$

¹The reader could note we only mention a model to compute the lift force - the force that acts in upward direction in a knuckleball throw - whereas the lateral force caused by the same effect is omitted. This is not far from the reality since the lateral coefficient of throws with 4S and 2S orientations is always close to zero by the symmetry of the seams [7].

In this way, $a_0 = b_0/2$ whereas $a_1 = 1/(2n)$, and thus, we calculate $b_0 = 0.3$ fits the Borg & Morrissey data.

The results for both methods, equation 4.8 and least-square, are plotted in Figure 4.2. In general, they are very similar between them and fit well to the experimental data. It can be mentioned that when experimental data and/or results are above the sine function (4.2) it means that there are more stitches close to the stagnation point from the down-side of the ball, and vice-versa. Thus, we observe that ball seams of 4S pitches have more symmetry than those with 2S orientation. In this way, the model shows the asymmetry of the front of the ball by means of the value of the lift coefficient (larger values correspond to a high level of asymmetry).

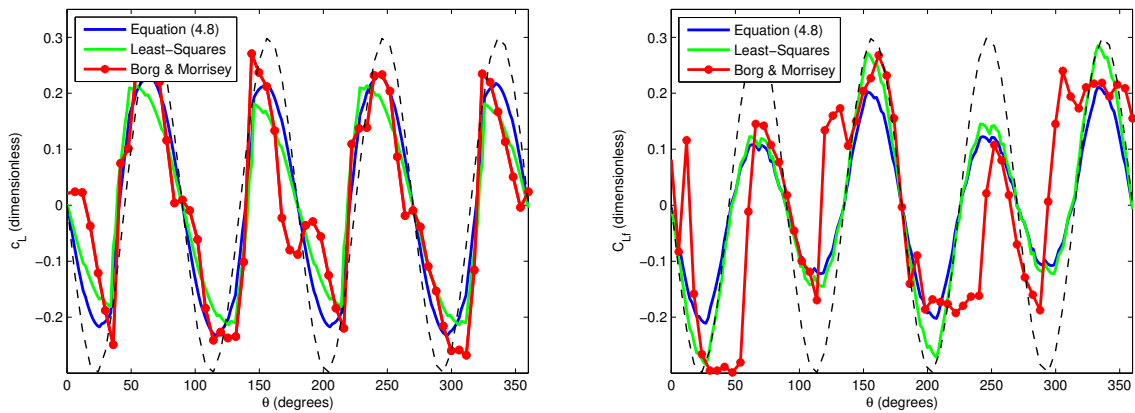


FIGURE 4.2: Lift coefficient c_L in function of the angle θ computed by (4.8), least-squares method and experimental data of Borg & Morrissey for non-spinning balls. Equation (4.2) with $a_0 = 0.3$ (black dashed line) is plotted as a baseline. Left: 4S orientation. Right: 2S orientation.

More precisely, both 4S models and experimental data look like the sine function (4.2) but with a fast-growing in convex parts and a smooth fall in concave ones, see the left-hand side of Figure 4.2. The models are very close to the data values, although a discrepancy is observed every 45° at the peaks of the oscillatory function, and every 90° when the function falls around the value of zero.

Such discrepancies can be explained by the effect of the stitches. We have computed them as a set of points that simulate a continue curve, however, the stitches have a width of about one centimeter, which represents 16° of the ball circumference, approximately. In this way, we aren't calculating the total effect of the seams since extra-turbulent flows are caused by the width of the stitches.

On the other hand, real data and results for 2S orientations indicate that the lift coefficient depends on the seams position as a periodic function with the same periodicity of the 4S orientation, but with different amplitudes, reflected and inverted about 180° . Both models seem to smooth out the real data although the adjustment is less accurate than for 4S orientation. Peaks of the least-square approximation are closer to the experimental data than the equation (4.8), spiting that one around the 210° . Main discrepancies are observed every 90° when the function grows, which also can be attributed to the pass of the stitches, see right-hand of Figure 4.2.

We obtain the stitch positions \mathbf{S} by modeling a baseball with a test version of Rhinoceros 5 program, following the tutorial video [44]. In this way, 2S and 4S models consider a set of 132 stitches ($n = 132$).

Knuckleball Trajectories

Simulation of knuckleball throws have been carried out for 4S and 2S ball orientations by using the lift force model (4.5) in (1.8) with ball and Earth parameters as in Section 2.2, and using equation (4.8) to compute the lift coefficient. We chosen the model (4.8) because it fits to the Borg & Morrissey data with the same values of b_0 for both ball orientations, although least squares approximation is the main method to consider.

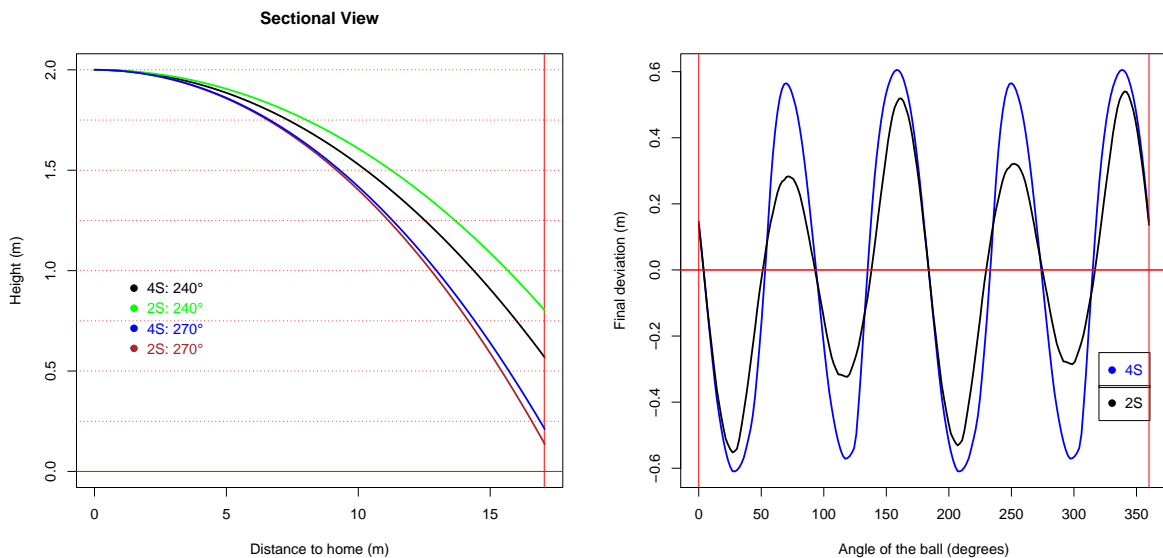


FIGURE 4.3: Knuckleball with an initial speed of 30 m/s thrown from an height of 2 m at different angles and orientations. Left: Four trajectories with different initial conditions. Right: Distance at home between the position of the ball and the expected final position (thinking on to compute equation (1.8) without lift force) for all angles in 4S and 2S orientations.

Figure 4.3 shows some trajectories with different initial angles in a sectional view (left-hand) and the deviation of the ball at home caused by the lift force (right-hand). An example of how the angle and the ball orientation determine a trajectory can be seen in left-hand graphic, in which a batter would see the same trajectory for both 4S and 2S orientation of a ball thrown with the initial angle of 270° , although the final position of the ball differs around 7 cm (approximately the diameter of the ball). Meanwhile, positions of a ball thrown with an initial angle of 240° are totally different throughout the trajectory for 4S and 2S orientations, which is also reflected at the final deflections with 30 cm of difference, approximately.

Moreover, 4S pitches can produce larger forces than balls with 2S orientations as seen in right-hand of Figure 4.3. Indeed, the graphic shows that both 4S and 2S types of pitches have the same oscillatory effect on a trajectory but differ only in larger deflections reached with 4S orientation.

Chapter 5

Conclusions

A method to reconstruct trajectories of spinning baseballs was designed, which requires only three ball positions. This is possible because the Magnus force can be separate from the rest of the forces that define the dynamics of a throw. The method is applied in an algorithm based on shooting method, which obtains the initial conditions of synthetic trajectories by minimizing the distance between data points of the original trajectory and those of the proposed trajectory. Results show the high accuracy of the algorithm in low computation time, even if it converges better with taking midpoints between one-third and the half of the trajectory. The methodology and the results of this research allow us to consider a possible comparison with future experiments and its compatibility in other areas. Stability analyses over physic and numerical parameters can be carried out in the future to justify the convergence of the algorithm.

Regarding knuckleballs, we develop a mathematical model to compute the coefficient of the lift force acting in upward direction for balls with 4S and 2S orientations. The model considers the effect of each stitch throughout the ball seams. In this way, the lift coefficient is computed in function of the initial angle of the ball. Computation is carried out in two ways, both of them reproduce experimental data reported in literature with only some disturbances seen every 45° and 90° for 4S and 2S orientations, respectively, which are due to the turbulent flows that are not considered in this work. Even so, the results match with the experimental data, which motivates us to compare the model with future experiments and to improve it by considering the assumptions mentioned above. We also propose to extend the model for different orientations and for balls spinning at low frequencies.

Finally, we mention that both works together contribute to understand the aerodynamics of baseballs but even more of any kind of ball flying with or without an initial spin.

Bibliography

- [1] Adair R.K., *The Physics of Baseball*, Harper-Collins Publishers, 3rd Edition, 2002.
- [2] Taylor J.R., *Classical Mechanics*, University Science Books, 1st Edition, USA, 2005.
- [3] Fitzpatrick R., *Theoretical Fluid Mechanics*, 2016. Online document available at <http://farside.ph.utexas.edu/teaching/336L/Fluid.pdf>.
- [4] Briggs L.J., Effect of Spin and Speed on the Lateral Deflection (Curve) of a Baseball; and the Magnus Effect for Smooth Spheres, *American Journal of Physics*, 27(589), 1959.
- [5] Nathan A.M, The effect of Spin on the Flight of a Baseball, *American Journal of Physics*, 76(2), 2008.
- [6] Robinson G., & Robinson I., The Motion of an Arbitrarily Rotating Spherical Projectile and its Application to Ball Games, *Physica Scripta*, 88, 018101 (17pp), 2014.
- [7] Borg J.P., & Morrissey M.P., Aerodynamics of the knuckleball pitch: Experimental measurements on slowly rotating baseballs, *American Journal of Physics*, 82(10), 2014.
- [8] Statistics of 2015 MLB games, <http://m.mlb.com/news/article/160896926/statcast-spin-rate-compared-to-velocity>
- [9] *Official Baseball Rules*, 2015 Edition, http://mlb.mlb.com/mlb/downloads/y2015/official_baseball_rules.pdf.
- [10] Hennekam W., The speed of a cyclist, *Physics Education*, 25, 1990.
- [11] Daish C.B., *The Physics of Ball Games*, The English Universities Press, 1972.
- [12] Kray T., Franke J., & Frank W., Magnus Effect on a Rotating Soccerball at High Reynolds Numbers, *Journal of Wind Engineering and Industrial Aerodynamics*, 124, 46–53, 2014.
- [13] Sayers A.T., & Hill A., Aerodynamics of a Cricket Ball, *Journal of Wind Engineering and Industrial Aerodynamics*, 79, 169-182, 1999.

-
- [14] Goodwill S.R., Chin S.B., & Haake S.J., Aerodynamics of Spinning and Non-Spinning Tennis Balls, *Journal of Wind Engineering and Industrial Aerodynamics*, 92, 935-958, 2004.
- [15] Halliday D., Resnick R., & Walker J., *Fundamentals of Physics*, Wiley, 9th Edition, 2011.
- [16] Theobalt Ch., Albrecht I., Haber J., Magnor M., & Seidel H.-P., Pitching a Baseball - Tracking High-Speed Motion with Multi-Exposure Images, ACM 0730-0301/04/0800-0540, 2004.
- [17] Robinson G., & Robinson I., Reply to Comment on 'The motion of an arbitrarily rotating spherical projectile and its application to ball games', *Physica Scripta*, 89, 067002, 2014.
- [18] Ward-Alaways L., *Aerodynamics of the Curve-Ball: An Investigation of the Effects of Angular Velocity on Baseball Trajectories*, Philosophy Doctoral Thesis, University of California, 1998, <http://biosport.ucdavis.edu/lab-members/leroy-alaways/Baseball.pdf>.
- [19] Regarding Knuckleballs, <http://www.physics.usyd.edu.au/~cross/KNUCKLEBALLS.htm>
- [20] Ranger K.B., Time-Dependent Decay of the Motion of a Sphere Translating and Rotating in a Viscous Liquid, *Quarterly Journal of Mechanics and Applied Mathematics*, 49(4), 1996.
- [21] Walsh J., Butterflies are not bullets, *The Hardball Times*, 2007.
- [22] Nathan A.M, Analysis of Knuckleball Trajectories, *Procedia Engineering*, 34, 116-121, 2012.
- [23] Watts R.G., & Sawyer E., Aerodynamics of a knuckleball, *American Journal of Physics*, 43(11), 1975.
- [24] Chang P., Han M., & Gong Y., Extract Highlights from Baseball Game Video with Hidden Markov Models, *International Congress of Imaging Processing*, 0-7803-7622-6/02, 2002.
- [25] Takahashi M., Fujii M., & Yagi N., Automatic Pitch Type Recognition from Baseball Broadcast Videos, *International Symposium on Multimedia*, 978-0-7695-3454-1/08, 2008.
- [26] Shun H., & Komura T., A Spatiotemporal Approach to Extract the 3D Trajectory of the Baseball from a Single View Video Sequence, *International Conference on Multimedia and Expo*, 1583-1586, 2004.

- [27] Chu W.-T., Wang Ch.-W., & Wu J.L., Extraction of Baseball Trajectory and Physics-Based Validation for Single-View Baseball Video Sequences, *International Congress on Multimedia and Expo*, 1424403677/06, 2006.
- [28] Hung M.-H., Hsieh Ch.-H., Event Detection of Broadcast Baseball Videos, *Transactions on Circuits and Systems for Video Technology*, 18(2), 2008.
- [29] Guézic A., Tracking Pitches for Broadcast Television, *Computing Practices*, 0018-9162/02, 2002.
- [30] Syamsuddin M.R., & Kwon Y.M., Simulation of Baseball Pitching and Hitting on Virtual World, *Physica Scripta*, 663-667, 2011.
- [31] Cross R., *Physics of Baseball & Softball*, Springer, 1st Edition, 2011.
- [32] Burden R.L., & Faires J.D., *Análisis Numérico*, Cengage Learning Inc., 9th Edition, 2013.
- [33] Schwartz M., *Principles of Electrodynamics*, Dover Publications Inc., 2014.
- [34] Turing A.M., Computing Machinery and Intelligence, *Mind*, 49, 1950.
- [35] Tenenbaum M., & Pollard H., *Ordinary Differential Equations*, Dover Publications Inc., 2014.
- [36] El-Sayed A.M.A., Nour H.M., Raslan W.E., & El-Shazly E.S., A study of projectile motion in a quadratic resistant medium via fractional differential transform method, *Applied Mathematical Modelling*, 39, 2829–2835, 2015.
- [37] White A.B., *Numerical Solution of Two-Point Boundary-Value Problems*, Philosophy Doctoral Thesis, California Institute of Technology, 1974, http://thesis.library.caltech.edu/421/1/White_AB_1974.pdf.
- [38] Keller H.B., *Numerical Methods for Two-Point Boundary-Value Problems*, Blaisdell, 1968.
- [39] Ascher U.M., Mattheij R.M.M., & Russell R.D., *Numerical Solution of Boundary Value Problems for Ordinary Differential Equations*, Society for Industrial and Applied Mathematics, 1995.
- [40] Eastlake C.H., An Aerodynamicist's View of Lift, Bernoulli, *The Physics Teacher*, 40, 2002.
- [41] Waltham C., Flight without Bernoulli, *The Physics Teacher*, 36, 1998. and Newton

-
- [42] Baumeister T., Avallone E. A. & Baumeister III T., *Manual del Ingeniero Mecánico*, McGraw-Hill, 2nd Edition, 1993.
- [43] Tveito A., Langtangen H.P., Nielsen B.F., & Cai X., *Elements of Scientific Computing*, Springer, 2010.
- [44] Tutorial Rhino 3D | Modelar Pelota de Beisbol (1/2), <https://www.youtube.com/watch?v=ihh1Mpw9tSU&list=LLLi4JIty0PabkpCYZ5yHEg&index=23>.